1 **Monophyly of Diverse Bigyromonadea and their Impact on Phylogenomic Relationships**

2 **Within Stramenopiles**

3

4 Anna Cho[a], Denis V. Tikhonenkov[a,b], Elisabeth Hehenberger[c,d] Anna Karnkowska[e], Alexander P.
5 Mylnikov[b], Patrick J. Keeling[a]

6

7 [a] Department of Botany, University of British Columbia, Vancouver V6T 1Z4, British Columbia,
8 Canada

9 [b] Papanin Institute for Biology of Inland Waters, Russian Academy of Science, Borok 152742,
10 Russia

11 [c] Ocean EcoSystems Biology Group, GEOMAR, Helmholtz Centre for Ocean Research, Kiel
12 24105, Germany

13 [d] Institute of Parasitology, Biology Centre, Czech Academy of Sciences, 370 05 České
14 Budějovice, Czech Republic

15 [e] Institute of Evolutionary Biology, Faculty of Biology, Biological and Chemical Research
16 Centre, University of Warsaw, Warsaw 02-089, Poland

17

18

21 **Abstract**

22   Stramenopiles are a diverse but relatively well-studied eukaryotic supergroup with

23   considerable genomic information available (Sibbald and Archibald, 2017). Nevertheless, the

24   relationships between major stramenopile subgroups remain unresolved, in part due to a lack of

25   data from small nanoflagellates that make up a lot of the genetic diversity of the group. This is

26   most obvious in Bigyromonadea, which is one of four major stramenopile subgroups but

27   represented by a single transcriptome. To examine the diversity of Bigyromonadea and how the

28   lack of data affects the tree, we generated transcriptomes from seven novel bigyromonada

29   species described in this study: *Develocauda condao*, *Develocanicus komovi*, *Develocanicus*

30   *vyazemskyi*, *Cubaremonas variflagellatum*, *Pirsonia chemainus*, *Feodosia pseudopoda*, and

31   *Koktebelia satura*. Both maximum likelihood and Bayesian phylogenomic trees based on a 247

32   gene-matrix recovered a monophyletic Bigyromonadea that includes two diverse subgroups,

33   Developea and Pirsoniales, that were not previously related based on single gene trees.

34   Maximum likelihood analyses show Bigyromonadea related to oomycetes, whereas Bayesian

35   analyses and topology testing were inconclusive. We observed similarities between the novel

36   bigyromonad species and motile zoospores of oomycetes in morphology and the ability to self-

37   aggregate. Rare formation of pseudopods and fused cells were also observed, traits that are also

38   found in members of labyrinthulomycetes, another osmotrophic stramenopiles. Furthermore, we

39   report the first case of eukaryovory in the flagellated stages of Pirsoniales. These analyses reveal

40   new diversity of Bigyromonadea, and altogether suggest their monophyly with oomycetes,

41   collectively known as Pseudofungi, is the most likely topology of the stramenopile tree.

42

43

44   **1. Introduction**

45   Stramenopiles (= Heterokonts) are one of the well-characterized members of the

46   eukaryotic supergroup SAR (**S**tramenopila, **A**lveolate, **R**hizaria) (Keeling and Burki, 2019).

47   Stramenopiles are very diverse, comprising photoautotrophs (i.e. heterokont algae in

48   ochrophytes), osmotrophic oomycetes and labyrinthulomycetes with a motile zoospore life-stage

49   (e.g. *Phytophthora* sp*., Pythium sp.,* and labyrinthulids), and, free-living phagotrophic

50   opalozoans (e.g. *Cafeteria roenbergensis, Cantina marsupialis*) that occupy a broad range of

51   environments (Cavalier-Smith and Chao, 2006; Cavalier-Smith and Scoble, 2013a; Kolodziej

52   and Stoeck, 2007; Stiller et al., 2009; Tsui et al., 2009). Stramenopiles can be largely classified

53   into two major groups: Gyrista consisting of Ochrophyta, Oomycota, and Bigyromonadea; and

54   Bigyra consisting of Sagenista and Opalozoa. A single species *Platysulcus tardus,* has also

55   recently been shown to be a basal stramenopile (Thakur et al., 2019). While there is a lot of

56   genomic data from stramenopiles, only a handful comes from phagoheterotrophs (Mitra et al.,

57   2016), despite them representing much of the diversity as well as being key outstanding

58   problems in resolving controversies in stramenopiles phylogeny (Burki et al., 2016; Derelle et

59   al., 2016; Leonard et al., 2018; Shiratori et al., 2017, 2015).

60   One such clade is the subphylum Bigyromonadea, which was proposed to include the

61   class Developea (Aleoshin et al., 2016) and order Pirsoniales (Cavalier-Smith, 1998). The

62   monophyly of the Bigyromonadea is essentially untested, since only small subunit rRNA (SSU)

63   data are known from all but a single species (the exception being *Developayella elegans*, for

64   which a transcriptome is available), and the two groups never branch together in SSU

65   phylogenies (Aleoshin et al., 2016; Cavalier-Smith and Chao, 2006; Kühn et al., 2004; Weiler et

66   al., 2020).

67   Developea are marine bacterivores, including *Developayella elegans* (Leipe et al., 1996;

68   Tong, 1995) and *Mediocremonas mediterraneus* (Weiler et al., 2020), and the marine

69   eukaryovore *Develorapax marinus* (Aleoshin et al., 2016). Pirsoniales are parasites of other

70   microbes, including *Pirsonia guinardiae* (Schnepf et al., 1990) and *P. punctigera* (Schweikert

71   and Schnepf, 1997). These parasites deploy a pseudopod to squeeze through the frustule girdles

72   of their diatom host, while the main cell body (auxosome) stays outside of the host. The invading

73   pseudopod then phagocytoses the host cytoplasm or chloroplasts forming a trophosome (food

74   vacuole), which is then transported out to the auxosome (Kühn et al., 2004; Schnepf et al., 1990).

75   The relationship of both groups to other stramenopiles is uncertain, and both have led to

76   hypotheses about the evolution of other related groups. For example, the eukaryovory of *D.*

77   *marinus* and its placement in rRNA trees has led to the hypothesis that it represents a model for a

78   phagoheterotrophic ochrophyte ancestor (Aleoshin et al., 2016), however its position in the tree

79   varies between grouping with ochrophytes (Leonard et al., 2018) or oomycetes (Noguchi et al.,

80   2016; Thakur et al., 2019). Pirsoniales have also been found branching as sister to ochrophytes

81   based on SSU rRNA trees (Aleoshin et al., 2016; Kühn et al., 2004), although once again not

82   consistently and without strong support.

83   To test for the monopoly of bigyromonads and more thoroughly examine their

84   relationship to other stramenopiles, we significantly increased the diversity of genomic data from

85   the group by adding transcriptomes from seven newly discovered species belonging to

86   Pirsoniales (*Pirsonia chemainus* nom. prov., *Koktebelia satura* nom. prov., and *Feodosia*

87   *pseudopoda* nom. prov.) and Developea (*Develocanicus komovi* n. gen. n. sp., *Develocanicus*

88   *vyazemskyi* n. sp., *Develocauda condao* n. gen. n. sp., and *Cubaremonas variflagellatum* n. gen.

89   n. sp.). The inferred 247-gene phylogenomic tree, reconstructed with various methods, recovered

90   for the first time the monophyly of the Bigyromonadea. Maximum likelihood (ML) recovered a

91   robust monophyly of Bigyromonadea and oomycetes, while Bayesian inference and topology

92   testing were inconclusive. We describe several new features of the seven bigyromonads, and

93   noted their resemblance with oomycete zoospores, and report the first observation of

94   eukaryovory in the flagellated stages of Pirsoniales. Overall, these findings indicate

95   bigyromonada and ooymcetes are most likely sisters, and suggest potential ancestral state of the

96   oomycetes resembling bigyromonada, including their ability to form auto-aggregates (=self-

97   aggregates) (Galiana et al., 2008; Hickman, 1970; Ko and Chase, 1973) and phagoheterotrophy.

98

99   **2. Materials and Methods**

100   **2.1 Sample collection, identification, and library preparation**

101   Strain Colp-23 (*Develocanicus komovi*) was obtained from the black volcanic sand on the

102   littoral zone of Maria Jimenez Beach (Playa Maria Jiménez), Puerto de la Cruz, Tenerife, Spain,

103   October 20, 2014. Strains Colp-30 (*Develocanicus vyazemskyi*) and Chromo-1 (*Koktebelia satura*)

104   were isolated from the near shore sediments on the littoral zone near T.I. Vyazemsky Karadag

105   Scientific Station, Crimea, May 2015. Strain Chromo-2 (*Feodosia pseudopoda*) was obtained from

106   the near shore sand on the littoral zone of the beach in the settlement Beregovoye, Feodosiya,

107   Crimea, June 24, 2017. Strain Colp-29c (*Develocauda condao*) was isolated from the near shore

108   sediments on the north-east part of Con Dao Island, South Vietnam, May 4, 2015. Strains

109   '*Pirsonia*-like' (*Pirsonia chemainus*) and Dev-1 (*Cubaremonas variflagellatum*) were obtained

110   from a sea water samples taken in the Strait of Georgia, British Columbia, Canada (123° 28'50"

111   W, 49°10'366" N) at 70 m and 220 m depths, respectively using a Niskin bottle, June 13, 2017.

112   The samples were examined on the third, sixth and ninth day of incubation in accordance

113   with methods described previously (Tikhonenkov et al., 2008). *Procryptobia sorokini* strain B-69

114   (IBIW RAS), feeding on *Pseudomonas fluorescens*, was cultivated in Schmaltz-Pratt's medium at

115   a final salinity of 20‰, and used as a prey for clones Colp-23, Colp-29c, Colp-30, Chromo-1,

116   Chromo-2, and '*Pirsonia*-like' (Tikhonenkov et al., 2014). Bacterivorous strain Dev-1 was

117   propagated on the *Pseudomonas fluorescens*, which was grown in Schmaltz-Pratt's medium.

118   Strains Colp-23, Colp-29c, and Dev-1 are currently being stored in a collection of live protozoan

119   cultures at the Institute for Biology of Inland Waters, Russian Academy of Sciences, however,

120   strains Colp-30, Chromo-1, Chromo-2, and '*Pirsonia*-like' perished after several months to one

121   year of cultivation.

122   Studied isolates were identified using a combination of microscopic and molecular

123   approaches. Light microscopy observations were made using a Zeiss AxioScope A.1 equipped

124   with a DIC water immersion objective (63x) and an AVT HORN MC-1009/S analog video camera.

125   The SSU rRNA genes (GenBank accession numbers: XXXXXX, XXXX…) were amplified by

126   polymerase chain reaction (PCR) using the general eukaryotic primers EukA-EukB (for strains

127   Colp-23, Colp-30, '*Pirsonia*-like'), PF1-FAD4 (Chromo-1), 18SFU-18SRU (Chromo-2, Dev-1),

128   25F-1801R (Colp-29c) (Cavalier-Smith et al., 2009; Keeling, 2002; Medlin et al., 1988;

129   Tikhonenkov et al., 2016). PCR products were subsequently cloned (Colp-23, Colp-30, Chromo-

130   2, '*Pirsonia*-like') or sequenced directly (Chromo-1, Dev-1, Colp-29c) using Sanger dideoxy

131   sequencing.

132   For cDNA preparation, cells grown in clonal laboratory cultures were harvested when

133   the cells had reached peak abundance (strains Colp-23, Col-30, Colp29c, Chromo-1, Dev-1) and

134   after the majority of the prey had been eaten (for eukaryovorous strains Colp-23, Col-30, Colp29c,

135   Chromo-1). Cells were collected by centrifugation (1000 x *g*, room temperature) onto the 0.8 µm

136   membrane of a Vivaclear mini column (Sartorium Stedim Biotech Gmng, Cat. No. VK01P042).

137   Total RNA was then extracted using a RNAqueous-Micro Kit (Invitrogen, Cat. No. AM1931) and

138   reverse transcribed into cDNA using the Smart-Seq2 protocol (Picelli et al., 2014), which uses

139   poly-A selection to enrich mRNA. Additionally, cDNA of Colp-29c was obtained from 20 single

140   cells using the Smart-Seq2 protocol (cells was manually picked from the culture using a glass

141   micropipette and transferred to a 0.2 mL thin-walled PCR tube containing 2 µL of cell lysis buffer

142   – 0.2% Triton X-100 and RNase inhibitor (Invitrogen)). The same 'single cell' transcriptomic

143   approach was applied for strains Chromo-2 and '*Pirsonia*-like', which never consumed the prey

144   completely. Sequencing libraries were prepared using NexteraXT protocol and sequencing was

145   performed on an Illumina MiSeq using 300 bp paired-end reads. Additionally, Chromo-1

146   transcriptome sequencing was performed on the Illumina HiSeq platform (UCLA Clinical

147   Microarray Core) with read lengths of 100 bp using the KAPA stranded RNA-seq kit (Roche) to

148   construct paired-end libraries. Raw reads are available in the NCBI Short Read Archive (SRA)

149   (Bioproject number: XXXXXX, SRAXXX-XXX).

150   **2.2 Small-subunit phylogenetic tree reconstruction**

151   SSU rRNA sequences were identified from the seven new assembled transcriptomes

152   using Barrnap v0.9 (Seemann, 2007) and compared with the SSU sequences obtained with

153   Sanger sequencing, and the longer sequences were used for further analysis.

154   After an initial BLASTn search of the SSU rRNA sequences against the non-redundant

155   NCBI database to confirm stramenopile identities, the SSU sequences were aligned using

156   MAFFT v7.222 (Katoh and Standley, 2013) with previously compiled SSU datasets (Aleoshin et

157   al., 2016; Yubuki et al., 2015). Additionally, SSU sequences of the other stramenopile taxa that

158   were included in the multi-gene phylogenomic dataset and other closely related taxa were

159   included in Fig. 3. Furthermore, to show the diversity of uncultured Gyrista and provide possible

160   directions for future sampling efforts, environmental sequences of stramenopiles that are closely

161   related to Pirsoniales and Developea were added in Fig. S4. After trimming using trimAl

162   v.1.2rev59 (-gt 0.3, -st 0.001) (Capella-Gutiérrez et al., 2009), the SSU phylogenetic trees were

163   reconstructed based on 1650 sites and 92 taxa for Fig. 3, and 1665 sites and 107 taxa for Fig. 4S,

164   using IQ-TREE v1.6.12 (Nguyen et al., 2015) 1000 ultrafast bootstrap (UFB) under Bayesian

165   information criterion (BIC): TIM2+R6 selected by ModelFinder (Kalyaanamoorthy et al., 2017)

166   implemented in IQ-TREE.

167   **2.3 Transcriptome processing, assembly, and decontamination**

168   Raw sequencing reads were assessed for quality using FastQC v0.11.5 (Andrews, 2010)

169   and remnant transposase-inserts from the library preparation were removed. The reads were

170   assembled using Trinity-v2.4.0 with *–trimmomatic* option to remove NexteraXT adaptors,

171   Smart-Seq2 IS-primer, and low quality leading and trailing ends (quality threshold cut-off:5)

172   (Bolger et al., 2014; Grabherr et al., 2011). To identify contaminants, assembled reads were

173   searched against the NCBI nucleotide database using megaBLAST (Basic Local Alignment

174   Search Tool) (Altschul et al., 1990), followed by diamond BLASTX against a UniProt reference

175   proteome (Bateman et al., 2021). To visualize the contig sizes, coverage, and remove bacterial,

176   archaeal, and metazoan contaminants, BlobTools v1.0 (Laetsch and Blaxter, 2017) was used.

177   PhyloFlash v3.3b2 (Gruber-Vodicka et al., 2020) was used in parallel to confirm identified

178   contaminants and coverage based on SILVA v138 SSU database (Quast et al., 2013). To remove

179   sequences from the prey, *Procryptobia sorokini,* which was used in the cultures of *Pirsonia*

180   *chemainus*, *Koktebelia satura*, *Feodosia pseudopoda*, *Develocanicus komovi*, *D. vyazemskyi*, and

181   *Develocauda condao*, the assembled reads were searched against the *P. sorokini* transcriptome

182   using BLASTn in which the contigs with ≥95% sequence identity were removed from the

183   assembled reads. To predict open reading frames (ORFs) and coding genes, TransDecoder v5.5.0

184   (Haas, 2015) was used and the longest ORFs were annotated using BLASTP search against

185   UniProt database. To estimate the completeness of each of the assembly, BUSCO v4.0.5 (Simão

186   et al., 2015) with eukaryotic database was used.

187   **2.4 Phylogenomic matrix construction and ortholog identification**

188   To better represent each stramenopile (sub)group in the phylogenomic reconstruction,

189   recently published and publicly available (Broad Institute and Japan Agency for Marine-Earth

190   Science and Technology; JAMSTEC) additional 27 stramenopile genomic or transcriptome data

191   (de Vargas et al., 2015; Hackl et al., 2020; Keeling et al., 2014; Leonard et al., 2018; Noguchi et

192   al., 2016; Seeleuthner et al., 2018; Thakur et al., 2019; Wawrzyniak et al., 2015) were obtained

193   and analyzed along with the seven new transcriptomes (Table S1). The updated stramenopile

194   dataset including all the newly added transcriptomes in this study were compiled to the existing

195   gene-set described below. Using BLASTP, the predicted coding genes from each transcriptome

196   were searched against 263 gene-sets (orthologs), each consisting of compiled genes from major

197   supergroups of protists, fungi, and holozoans (Burki et al., 2016; Hehenberger et al., 2017). The

198   search results were filtered with an e-value threshold of 1e-20 with >50% query coverage,

199   followed by read trimming based on UniProt search results. Each gene-set was aligned using

200   MAFFT-L-INS-i v.7222 and trimmed using trimAL v1.2rev59 (-gt 0.8). To identify orthologs

201   from the newly added transcriptomes aligned to the corresponding 263 gene-sets, 263 gene-trees

202   were built using Maximum-likelihood (ML) estimation with IQ-TREE v1.6.12 under the

203   LG+I+G4 model and 1000 ultrafast bootstrap (UFB) approximation. Each gene tree was

204   manually screened in FigTree v1.4.4 and searched against BLAST nr-database for paralogs and

205   contaminants (e.g., long branching sequences or sequences nested within bacterial, opisthokont

206   and other distantly related clades), which were subsequently removed from each of the gene-set

207   alignment. To increase ortholog coverage from the added transcriptomes, fragmented orthologs

208   were manually combined only when the fragments were positioned in the same clade in a given

209   gene tree, covered different regions of a gene, and if there was an overlapping region present,

210   permitting up to two mismatches. The 263 gene-sets containing the selected orthologs of the

211   newly added transcriptomes and 27 newly published stramenopile data were aligned using two

212   approaches and compared by reconstructing two phylogenomic trees. In the first approach

213   (**approach 1**), the sequences were aligned by using MAFFT L-INS-i v.7.222 and trimmed via

214   trimAL v1.2rev59 (-gt 0.8). In the second approach (**approach 2**), the sequences were filtered

215   using PREQUAL (Whelan et al., 2018) to remove non-homologous regions generated due to

216   poor transcriptome quality or assembly errors. The filtered sequences were then aligned using

217   MAFFT G-INS-i (--allowshift and --unalignlevel 0.6 option) and processed for further filtering

218   using Divvier (-mincol 4 and -divvygap option) (Ali et al., 2019) to identify statistically robust

219   pairwise homology characters. The filtered gene-sets were then soft-trimmed using trimAL (-gt

220   0.1). The two dataset generated by two different filtering and alignment methods were separately

221   processed using SCaFoS v1.2.5 (Roure et al., 2007), by removing gene-sets that have ≥40%

222   missing amino acid positions in the alignment. The resulting 247 gene-set was concatenated into

223   a phylogenomic matrix comprising 75,798 amino acid (aa) sites from 76 taxa for approach 1. For

224   the PREQUAL/Divvier processed data (approach 2), the same 247 gene-sets were concatenated

225   in a phylogenomic matrix comprising 101,314 aa sites from the same 76 taxa.

226   **2.5 Phylogenomic tree reconstruction, fast-evolving site removal, and topology test**

227   The ML tree for the concatenated phylogenomic matrix was inferred using IQ-TREE

228   v.1.6.12 under the empirical profile mixture model, LG+C60+F+G4 (Quang et al., 2008). The

229   best tree under this model was used as a guide tree to estimate the "posterior mean site

230   frequencies" (PMSF). The PMSF method allows the conduction of non-parametric bootstrap

231   analyses under complex models on large data matrices and was shown to mitigate long-branch

232   attraction artifacts (Wang et al., 2018). This LG+C60+F+G-PMSF model was then used to re-

233   estimate the ML tree and for a non-parametric bootstrap analysis with 100 replicates. For

234   Bayesian inference, CAT-GTR mixture model with four gamma rate categories was used with

235   PhyloBayes-MPI v.20180420 (Lartillot et al., 2009; Lartillot and Philippe, 2004), only for the

236   dataset processed with approach 1. To estimate posterior probability, four independent Markov

237   Chain Monte Carlo (MCMC) chains were run simultaneously for minimum 10,000 cycles. After

238   discarding the first 2000 burn-in points, consensus posterior probability and topology were

239   computed by subsampling every second tree. Convergence of the four chains were tested by

240   calculating differences in bipartition frequencies (bpcomp) with a threshold maxdiff however, no

241   chains converged (maxdiff=1).

242   Site-specific substitution rates were inferred using the -wsr option as implemented in IQ-

243   TREE, under the LG+C60+F+G4 substitution model. Increments of the top 5% fastest evolving

244   sites were removed (Irwin, 2021) from the phylogenomic matrix until exhaustion, defined as the

245   point when the bootstrap support value significantly began to drop and the topology became

246   unstable (50%; 37,899 sites). Each incremental phylogenomic matrix was analyzed using IQ-

247   TREE for ML estimation using LG+C60+F+G4 and 1000 UFB. All fast-evolving species

248   removal and sites tests were conducted on the dataset processed with approach 1.

249   Approximately unbiased (AU) tests (Nguyen et al., 2015; Shimodaira, 2002) were

250   performed on set of phylogenomic trees constructed based on the 247 gene-sets generated by the

251   first approach (i.e., MAFFT L-INS-i and trimAL with -gt 0.8) and the second approach (i.e.,

252   PREQUAL/Divvier), separately. The set of trees includes the two ML trees generated under

253   LG+C60+F+G4(+PMSF) with 1000UFB (100STB), four consensus trees of MCMC chains, and

254   other hypothetical constrained trees as listed as "Chain modified" in Table 1.

255   **3. Results**

256   **3.1 Multi-gene phylogenomic analysis**

257   The concatenated phylogenomic matrix was composed of 68 stramenopiles and eight

258   alveolates (outgroup) with 247 aligned genes totaling 75,798 positions for approach 1, and

259   101,314 positions for approach 2. The average missing sites and genes were 22% and 19%,

260   respectively (Fig. 1). The amount of missing data varied among the seven new transcriptomes.

261   Chromo-1 had nearly complete data (5% missing sites and 6% missing genes) while Colp-29c

262   had 21% missing sites and 12% missing genes. Colp-23 and Chromo-2 had the highest amount

263   of missing data (75% missing sites and 57% genes for Chromo-2 and, 83% and 76% for Colp-

264   23). The ML phylogenomic tree generated under LG+C60+F+G4+PMSF with STB estimation

265   from the two approaches is shown in Figure 1, with the tree topology representing the dataset

266   generated from approach 1 (i.e., MAFFT L-INS-i and trimAL with -gt 0.8). The tree topology

267   representing the dataset generated from approach 2 (i.e., Prequal/Divvier) is shown in Figure S1.

268   The tree topology is almost identical between the two, except the position of sub-clades in

269   ochrophytes; for example, the positions of Chrysophyceae + Synurophyceae and

270   Raphidophyceae + Phaeophyceae + Xanthophyceae + Eustigmatophaceae are swapped in the

271   two trees (Fig. 1; Fig. S1).

272   The newly added transcriptomes of the seven new species formed the robust

273   monophyletic bigyromonada with either dataset (approach 1 and approach 2; Fig. 1; Fig. S1):

274   *Develocanicus komovi*, *D. vyazemskyi*, *Develocauda condao,* and *Cubaremonas variflagellatum*

275   forming a Developea clade (100% STB), while Pirsoniales is composed of *Pirsonia chemainus*,

276   *Koktebelia satura*, and *Feodosia pseudopoda* (100% STB). The ML tree also recovered

277   monophyly of the bigyromonada and oomycetes with 100% STB support (Fig. 1). The

278   monophyly of Gyrista was strongly supported, with Sagenista (Labyrinthulomycetes and

279   Eogyrea) forming a sister clade to it, resulting in a paraphyletic Bigyra. Platysulcea formed a

280   sister clade to rest of the stramenopiles with a moderate support (91%/95% STB) (Fig.1; Fig.

281   S1).

282   Bayesian analyses recovered a conflicting topology for the bigyromonada, which formed

283   a sister-clade to ochrophytes in all four consensus trees generated (Fig. S2). Additionally, the

284   topology within ochrophytes was inconsistent, preventing convergence. However, the

285   monophyly of bigyromonada + ochrophytes was rejected by approximately unbiased (AU) tests

286   in three of the four consensus trees. AU test failed to reject the chain 1 consensus tree at a

287   confidence interval of 95% (p-AU $\geq$ 0.05) (Fig. S2). Interestingly, the sub-clade topology of

288   ochrophytes in chain 1 is the same as in the ML phylogenomic tree generated using the approach

289   1 (Fig. 1; Fig. S2). When the AU tests were repeated on hypothetically constrained trees where

290   bigyromonada + oomycetes were monophyletic but the rest of the topology was unchanged for

291   each of the MCMC chains, the tests failed to reject the monophyly of bigyromonada +

292   oomycetes (Table 1). Rejection of bigyromonada + ochrophytes was also observed in

293   constrained trees when the AU test was repeated on the dataset processed with approach 2 (Table

294   S2). To evaluate the effect of fast-evolving sites, bootstrap support and topology were compared

295   among the ML trees that were reconstructed with increments of 5% fast-evolving sites removed

296   from the dataset processed with approach 1. The topologies of the phylogenomic tree were

297   maintained while the UFB support for Platysulcea increased up to 97% (Fig. 2). To account for

298   possible artefacts due to long-branching attraction of fast-evolving species, tree reconstruction

299   was repeated after removing *Cafeteria roenbergensis*, the two *Blastocystis* species, and *Cantina*

300   *marsupialis*. The monophyly of bigyromonada and oomycetes was recovered with 85% UFB,

301   however the topology of Bigyra became unresolved with weak support for its monophyly (Fig.

302   S3)

303   **3.2 Small-subunit ribosomal RNA gene tree reveals two different species assigned as**

304   ***Developayella***

305   As shown previously, the SSU rRNA phylogenetic tree recovered the bigyromonada as

306   paraphyletic group, with the Pirsoniales (*Pirsonia chemainus*, *Koktebelia satura*, and *Feodosia*

307   *pseudopoda*) forming a sister clade to ochrophytes (92% UFB) while the Developea clade was

308   recovered as sister to oomycetes (Fig. 3). Within the Developea clade, in addition to the SSU

309   rRNA sequences obtained from *Cubaremonas variflagellatum* and the JAMSTEC *Developayella*

310   *elegans* transcriptome, we included three publicly available SSU rRNA sequences assigned as

311   *Developayella* spp.: Accession ID U37107 (Leipe et al., 1996; Tong, 1995), MT355111.1

312   (Unpublished) and JX272636.1 (Del Campo et al., 2013): (note: although JX272636.1 is

313   assigned as "Cf. *Developayella* sp." in GenBank, it was recently re-assigned as *Mediocremonas*

314   *mediterraneus* (Weiler et al., 2020)). Interestingly, the SSU rRNA sequences of the four

315   "*Developayella*" fell into two separate groups, indicating two different species (and genera) were

316   assigned as *Developayella elegans*; sub-clade I consisted of *Developayella elegans* U37107,

317   *Developayella* sp. MT355111.1, *Develocanicus komovi*, *D. vyazemskyi*, and *Develocauda*

318   *condao,* while sub-clade II consisted of *M. mediterraneus* (JX272636.1 and MT918788.1),

319   JAMSTEC *Developayella elegans*, and *Cubaremonas variflagellatum* (Fig. 3). The SSU rRNA

320   sequence similarity between the two sub-clade I *Developayella* species (U37107 and

321   MT355111.1) is 98.987%, between the two species (JAMSTEC *D. elegans* and *Cubaremonas*

322   *variflagellatum*) in sub-clade II 97.528% and between the originally described *Developayella*

323   *elegans* U37107 and *Cubaremonas variflagellatum* 91.143%.

324   **3.3 Morphology of the novel species**

325   Developea Karpov et Aleoshin 2016

326   ***Develocanicus vyazemskyi* (Fig. 4A, B) and *Develocanicus komovi* (Fig. 4C–M)**

327   Free-swimming naked eukaryovorous heterokont flagellates. The shape of the cell is

328   irregularly flattened ellipse, where the dorsal side is more convex, and the ventral side is flatter.

329   Two species differ in size, *Develocanicus vyazemskyi* (Colp-30) is larger and rounder, 7.4 - 12.5

330   μm long, 4.8 - 9.2 μm wide, typical dimension ranging 9.2 x 7.0 μm. *Develocanicus komovi* (Colp-

331   23) is slightly smaller, with the length 5.4 - 10 μm, width 3.8 - 7.4 μm and a typical dimension of

332   7.1 x 5.1 μm.

333   Cell possesses two non-acronematic heterodynamic flagella of unequal lengths (Fig. 4A-

334   D, F, I, J). The posterior flagellum is two times longer than the cell, the anterior flagellum is

335   approximately 1 - 1.5 times longer. Flagella emerge from a prominent ventral depression (Fig. 4A-

336   D) which passes into a shallow wide groove (Fig. 4E) along the entire length of the cell. Cells

337   predominantly exhibit active and quick swimming without rotation. During swimming, the

338   posterior flagellum is directed backward and straight, running along the ventral depression of the

339   cell. The anterior flagellum beats rapidly and is directed forward while slightly curved. In non-

340   motile cells, both flagella are directed backward, beating in a slow sinusoidal wave (Fig. 4G, J).

341   The medial nucleus is located closer to the dorsal side of the cell (Fig. 4H). A large

342   digestive vacuole is situated at the posterior part of the cell (Fig. 4I, J). As it is digested, the

343   posterior end of the cell becomes thinner. The cells can form aggregations and attach to each other

344   (Fig. 4K), sometimes form pseudopodia (Fig. 4L). Transverse binary fission (Fig. 4M).

345   ***Develocauda*** *condao* (**Fig. 4N–W**)

346   Free-swimming eukaryovorous heterokont flagellates (Colp-29c). The cells are slightly

347   flattened, usually elongated-oval, less often narrow-oval or almost rod-shaped (Fig. 4Q). The

348   anterior end is more rounded, the posterior end of the cell can be pointed, forming a

349   characteristic "tail" found in starving cells (Fig. 4R, S). Cell length 5.14 - 12 μm, width 2.8 -

350   5.42 μm typically ranging 7.14 x 4.28 μm in dimension. The caudal extension is about 4.57 x

351   1.42 μm in size.

352   The cells have two heterodynamic flagella of an almost equal length with a posterior

353   flagellum compared to the cell body. Flagella emerge from a pronounced deep ventral depression

354   (Fig. 4N, O), which almost extends to the dorsal side of the cell. Depression transforms into a

355   shallow groove (Fig. 4P) spanning along the entire cell, in which the posterior flagellum can fit.

356   The cells swim very quickly without rotating along the longitudinal axis. The posterior

357   flagellum is straight and directed backwards. The anterior flagellum is directed forward, beats

358   actively, and is only slightly curved. Rarely, the cells lie at the bottom with both flagella directed

359   backward while making a slow sinusoidal movement, or the posterior flagellum beating actively.

360   The aggregated (Fig. 4U), partially fused cells (Fig. 4W) that form clusters were observed

361   in culture. The medial nucleus is located closer to the dorsal side of the cell. Sated cells do not

362   have a tail; at the posterior end of their cells there is a large digestive vacuole (Fig. 4T). Transverse

363   binary fission (Fig. 4V).

364   *Cubaremonas variflagellatum* **(Fig. 4X–AE)**

365   Cells (clone Dev-1) are naked and solitary bacteriovores with the length 3.7 - 8 μm, the

366   width 2.6 - 5.4 μm, and the typical dimension of 5.0 x 3.7 μm. The cell shape varies from

367   elongated oval, oviform to rounder form (Fig. 4X-AA). Typically, the shape is irregularly ovoid,

368   with the convex dorsal side and the flatter ventral side. The shape and size vary depending on

369   feeding conditions. Starving cells have a small rostrum at the anterior end (Fig. 4AD). Cells are

370   larger before division.

371   The cells possess two heterodynamic flagella of unequal length, emerging from a

372   conspicuous ventral depression (Fig. 4Z, AB). Ventral depression starts from the anterior tip and

373   continues ventrally to the middle of the cell. The anterior flagellum is approximately equal to the

374   cell length or slightly longer while the posterior flagellum is 1.5 - 1.8 times longer than the cell.

375   Digestive vacuole is situated at the cell posterior. An observed cell division produces two or four

376   cells (Fig. 4AE).

377   In culture condition, the cells predominantly lie at the bottom unattached with both

378   flagella directed backward. The posterior flagellum runs along the ventral surface of the cell and

379   beats rapidly with sinusoidal pattern to draw water through the depression. The anterior

380   flagellum is hook-shaped and sweeps slowly down behind the posterior flagellum.

381   Although less common, when the cells swim, the curved anterior flagellum actively beats,

382   pulling the cell forward. It is almost invisible due to its fast beating. The posterior flagellum

383   extends behind the cell and is likely used as a rudder. The cells swim quickly, only occasionally

384   rotating about the axis of motion. Cells can sharply change the direction of movement.

385

386   Pirsoniales Cavalier-Smith 1998 emend. 2006

387   *Feodosia pseudopoda* **(Fig. 4AF, AG, AJ–AS),** *Koktebelia satura* **(Fig. 4AH), and**

388   *Pirsonia chemainus* **(Fig. 4AI).**

389   Free-swimming naked, solitary and eukaryovorous heterokont flagellates. Cells are shaped

390   as a flattened oval, with slightly pointed ends with the size 10.5 - 14 μm in length, 6 - 9.1 μm in

391   width, and typically having the dimension of 12 x 8.2 μm. The flagellated stages of three studied

392   Pirsoniales were almost morphologically identical except *Feodosia pseudopoda* (Chromo-2)

393   which possesses small notch at the anterior part of the cell (Fig. 4AF, AG). Rarely, *F. pseudopoda*

394   can produce pseudopodia (Fig. 4AM, AN), which are up to 10 μm long and sometimes branched.

395   Two long heterodynamic flagella originate from the pit located in the anterio-medial part

396   of the cell (Fig. 4AL, AM, AO). The length of the anterior flagellum is as long as the cell, while

397   the posterior one is 2.5 times longer.

398   The cells swim fast in a straight line, without rotating along the longitudinal axis. The

399   anterior flagellum is directed anteriorly, always bent towards the ventral surface. The posterior

400   flagellum propels the cell and beats at a high speed, which can be seen as multiple posterior flagella

401   (Fig. 4AI). In stationary cells, the flagella take the form of a sinusoid (Fig. 4AJ, AK).

402   The nucleus is located in the middle of the cell (Fig. 4AJ). The cytoplasm contains many

403   refractive granules as observed in previously described *Pirsonia* species (Schweikert and Schnepf,

404   1997). Non-flagellated cells were also observed with slightly amoeboid and round shape (Fig.

405   4AP–AR). The satiated cells have a large digestive vacuole at the posterior end (Fig. 4AS). The

406   eukaryovory of the biflagellates seems to be facultative as the most did not actively pursue the

407   prey but only *Koktebelia satura* (clone Chromo-1) consumed all the prey cells in culture.

408

409   **4. Discussion**

4.1 Monophyly and Phylogenetic Position of the Bigyromonadea

Of the known subdivisions of stramenopiles, the Bigyromonadea stand out for their lack of data and contentious position in the tree (even the newly discovered *P. tardus* is represented by transcriptomic data and consistency branches at the base of the tree). From the five recent phylogenomic analyses of stramenopiles, only three included a single bigyromonada representative (*D. elegans* JAMSTEC), none tested the monophyly of the group, and they recovered inconsistent positions. Using transcriptomes of seven new species belonging to the Bigyromonadea representing both the Developea and Pirsoniales subgroups, we tested the monophyly of the group and its position relative to other stramenopiles.

Previously, only SSU rRNA phylogenies could be used to test the monophyly of the Bigyromonadea, and such analyses consistently failed to support the monophyly, typically showing Developea with oomycetes and Pirsoniales with ochrophytes (Aleoshin et al., 2016; Kühn et al., 2004; Weiler et al., 2020). In contrast, phylogenomic data consistently and strongly supports the monophyly of these two groups, and shows each to include multiple distinct genera.

The position of Bigyromonadea within stramenopiles as a whole is also contentious, with some analyses showing the previously available transcriptome from *D. elegans* branching with oomycetes (Noguchi et al., 2016; Thakur et al., 2019), and based on internode consistency analyses (Kobert et al., 2016; Leonard et al., 2018, with ochrophytes). This discrepancy is not entirely eliminated by the addition of new taxa, since ML phylogenomic trees with the expanded representation recovered monophyly of the bigyromonada and oomycetes with robust support, but Bayesian analyses show a monophyly of bigyromonada+ochrophytes, and AU tests rejected most but not all topologies with this relationship (Table 1; Table S2).

432   The discrepancy between the ML and Bayesian analyses may be due to two groups

433   (Chrysista and Bigyromonadea) that do not fit the same model for tree reconstruction. Although

434   it is not the aim of this study to resolve the phylogeny of ochrophytes, further examination of

435   ochrophyte phylogeny, may reveal whether the discrepancy stems from the unreconciled model

436   used in the two groups, the different data processing approaches used, or insufficient data in one

437   or both groups.

438   These results change how we interpret these lineages and their biological characteristics

439   within the wider evolution of stramenopiles. For example, the phylogenetic position of

440   Pirsoniales inferred from ribosomal genes showed they share a recent common ancestor with the

441   ochrophytes, which naturally affected the interpretation of the ancestral state of ochrophytes and

442   the role of phagoheterotrophy in their evolution (Aleoshin et al., 2016; Shiratori et al., 2017).

443   However, the phylogenomic tree points instead to a phagoheterotrophic origin of the

444   Pseudofungi. Parallels between this and recent suggestions on the origin of fungi are noteworthy,

445   since *Paraphelidium tribonemae*, a phagoheterotrophic parasite belonging to phylum Aphelida,

446   has recently been found to be sister to the osmotrophic "core" fungi by phylogenomics (Torruella

447   et al., 2018). Close similarities in metabolism and a phagotrophy-related proteome profile of *P.*

448   *tribonemae* and the osmotrophic "core" fungi suggested the "core" fungi have evolved from a

449   phagoheterotrophic aphelid-like ancestor. Further information on the metabolism and feeding

450   mechanisms of the new species should shed light on whether the origins of fungi and

451   pseudofungi have more parallels and on the possible phagoheterotrophic ancestral state of

452   Gyrista more widely.

453   Of course, this is also dependent on conclusively determining the position of

454   Bigyromonadea. Substantial advances in phylogenetic methods have been made, but challenges

455   stemming from systematic errors, compositional bias, or long branch attraction, incomplete or

456   contaminated data, and models that do not account for heterotachy in large datasets (Delsuc et

457   al., 2005; Kapli et al., 2020; Zhou et al., 2007) remain. Similarly, advances in single-cell

458   sequencing have vastly increased the taxonomic scope of phylogenomics, but the severely

459   limited starting material and the fact that they are by definition a snapshot of gene expression in

460   one cell remain important hurdles. Here, the removal of fast-evolving sites (Fig. 2), species (Fig.

461   S3), extensive AU test (Table 1;Table S2;Fig. S2) and two different data processing approaches

462   collectively tip the scale in favour of the monophyly of bigyromonada and oomycetes over the

463   alternative position of bigyromonada with ochrophytes. However, the conflicting results of

464   Bayesian inferences show that the lack of a robust phylogenomic tree was not just due to lack of

465   taxonomic diversity. Continued sampling efforts in phagoheterotrophic stramenopiles will

466   expand the phylogenetic diversity of the Bigyromonadea (and environmental SSU rRNA data

467   already show there are more new taxa to be found), but other advances in data generation and

468   analyses will also be required.

469   **4.2 Morphology, evolutionary implications, and taxonomic description of the novel**

470   **phagoheterotrophic Bigyromonadea**

471   **4.2.1 Newly observed morphological and behavioural features in bigyromonads:**

472   **cell-aggregation to fusion, pseudopod-formation, and facultative phagotrophy in motile**

473   **zoospores**

474   Before we compare morphological features, we need to clarify that the JAMSTEC strain

475   of *Developayella elegans* has been mis-named and is a distinct species in a different genus.

476   According to the SSU rRNA gene tree (Fig. 3), the originally described *D. elegans* U37107

477   (Tong, 1995), is only distantly related to *D. elegans* JAMSTEC, and placed in distinct sub-clade

478   of Developea where it is most closely related to *C. variflagellatum*. Renaming *D. elegans*

479   JAMSTEC will be necessary in the future: its close relatedness to *Cubaremonas* is sufficient to

480   say it is mis-named, but rectifying this should take into account morphological information,

481   which is currently unavailable. Overall, however, the novel developeans have similar

482   morphological traits as previously described species. For example, *C. variflagellatum* falls in the

483   same sub-clade as *Mediocremonas mediterraneus* (Del Campo et al., 2013; Weiler et al., 2020)

484   (Fig. 3), and both have similar morphology. *C. variflagellatum* is slightly larger, but

485   measurements for *M. mediterraneus* (2.0 - 4.0 µm in length and 1.2 - 3.7 µm in width) were most

486   likely based on scanning electron microscopy (SEM) images and cells tend to shrink in SEM

487   fixatives (Weiler et al., 2020). The cell size, flagella length and swimming movement of *C.*

488   *variflagellatum* exhibited close similarity to *D. elegans* U37107, which was named after its

489   characteristic developpé movement of the anterior flagellum during stationary feeding (Tong,

490   1995). However, no thread-like substances were observed, which *D. elegans* uses to attach to

491   substrate.

492   The remaining novel Developea species, *Develocanicus vyazemskyi, D. komovi*, and

493   *Develocauda condao,* differed from *D. elegans* JAMSTEC and *C. variflagellatum* by having a

494   proportionately longer posterior flagellum, forward propulsion without rotating its axis, a

495   eukaryovorous diet (like *Develorapax marinus* (Aleoshin et al., 2016)), and the presence of a

496   "tail" in *D. condao*. Notably, the ability of the cells to form aggregates (Fig. 4K, U), pseudopodia

497   (Fig. 4L), and to undergo partial cell fusion (Fig. 4W) has not been reported in this clade

498   previously. The above-mentioned differences between *D. vyazemskyi D. komovi*, *Develocauda*

499   *condao*, and *C. variflagellatum* are also phylogenetically reflected in the division of these species

500   into two sub-clades (Fig. 1; Fig. 3).

501   The three novel Pirsoniales, *Feodosia pseudopoda, Koktebelia satura*, and *Pirsonia*

502   *chemainus,* described here as *nomen provisorium,* most likely represent a motile zoospore stage

503   of unknown algal parasites. The novel Pirsoniales species did not actively pursue the provided

504   prey and only partially consumed their prey (except *K. satura* which consumed all the prey

505   provided), all the cultures died after a few months to one year of cultivation. Although there has

506   been extensive description of auxosome and trophosome formation during the parasitic stage of

507   known Pirsoniales (Schnepf et al., 1990; Schweikert and Schnepf, 1997), the ability of motile

508   zoospores to acquire effective eukaryovory has not been described so far. The observed

509   eukaryovory of the zoospore-like Pirsoniales is likely facultative, as the cells were cultured

510   without potential hosts and the cells with larger food vacuoles became non-flagellated and

511   rounded, a structure akin to an auxosome. However, further culture experimentations with their

512   natural hosts are required to verify their ability to form parasitic auxosomes and trophosomes

513   from motile phagotrophic zoospores.

514   We postulate that the facultative eukaryovory at the motile zoospore stage provides a

515   significantly increased survival rate and thus extension of the motile stage during their dispersal

516   until a suitable host is found. This ability can be particularly advantageous before the onset of

517   seasonal algal bloom, where the zoospores can efficiently infect multiple hosts without resource

518   competition. Therefore, the sustained survival of the zoospores via facultative eukaryovory could

519   be an important factor leading to the evolutionary success of Pirsoniales parasites.

520   *Feodosia pseudopoda* differed from rest of the Pirsoniales studied here by an anterior

521   notch (Fig. AF, AG) and rare occurrences of pseudopodia (Fig. AM-AO). Interestingly, the two

522   characteristics have been reported in *Pseudopirsonia mucosa*, a cercomonad rhizarian (Kühn et

523   al., 2004), which had been mis-assigned as *Pirsonia* due to the similarities in their parasitic life

524   cycles. In starving and immobile zoospores of *Pirsonia puntigerae*, filopodium-like processes

525   (Schweikert and Schnepf, 1997) have been described however, pseudopodia in motile zoospores

526   of Pirsoniales have not been observed previously.

527   The presence of pseudopodia, and the ability to form aggregated cells in the newly

528   described sub-clade I of Developea and previously reported publications of Pirsoniales may

529   indicate synapomorphic traits of Bigyromonadea. It will be important for future studies to

530   compare ultrastructure and genes putatively associated with cell-aggregation or fusion among the

531   species of bigyromonada, thus potentially addressing the evolution of an osmotrophic nutritional

532   strategy in stramenopiles.

533   **4.2.2 Similarities among Oomycetes motile zoospores, Labyrinthulomycetes, and**

534   **Bigyromonadea**

535   Morphologically, the novel Developea species have similar features as motile zoospores

536   of previously studied oomycetes, such as the general cell dimension, the proportion between

537   anterior and posterior flagellum, and two laterally oriented flagella (with a tinsellate anterior

538   flagellum) emerging from a ventral groove (Dick, 2000), which resembles the ventral depression

539   observed in the novel species. Behaviourally, the swimming pattern (e.g., direction of flagella,

540   sinusoid form) is comparable (Hickman, 1970; Ho and Hickman, 1967). Another striking

541   similarity between the two groups is their ability to self-aggregate, which is observed in

542   oomycete zoospores as a distinct form of self-aggregation compared to aggregation towards host-

543   plant tissues (Bassani et al., 2020; Ko and Chase, 1973). The mechanism underlying self-

544   aggregation in oomycetes has not been fully resolved, however recent studies suggest that a

545   combination of chemotaxis (Bassani et al., 2020; Judelson and Blanco, 2005; Zheng and

546   Mackrill, 2016) and bioconvection (Savory et al., 2014), is involved in the process. The exact

547   role of the self-aggregation in oomycete pathogenesis is still unclear, however the fact that a

548   similar observation was made in its sister-clade, the Bigyromonadea, indicates that self-

549   aggregation may have been present in the ancestor of Pseudofungi, before the osmotrophic

550   parasitism of oomycetes evolved. Cell aggregation is also observed in *Sorodiplophrys* (Dykstra

551   et al., 1975), a species belonging to another osmotrophic group of stramenopiles, the

552   labyrinthulomycetes. Cell aggregation has convergently evolved multiple times across many

553   other supergroups (Parfrey and Lahr, 2013), such as Amoebozoa (Du et al., 2015), Rhizaria

554   (Brown et al., 2012), and ciliates (Sugimoto and Endoh, 2006), and whether cell aggregation

555   within stramenopiles arose convergently or divergently should be further investigated.

556   As mentioned previously, some species described in this study formed pseudopodia (Fig.

557   4L,4AM,4AN) and partially fused cells (Fig. 4W) resembling amoeboid forms. Interestingly,

558   labyrinthulomycetes also form filose pseudopodia (Gomaa et al., 2013) akin to pseudopodia

559   observed in this study (Fig. 4AM, AN). These are found in Amphitremidae, during an amoeboid

560   stage of *Diplophrys* (Anderson and Cavalier-Smith, 2012), and other labyrinthulids

561   (Raghukumar, 1992), implying this trait either evolved convergently or was present earlier than

562   the divergence of Pseudofungi.

563   Another notable similarity between oomycetes and the novel bigyromonada is their

564   potential marine origin, as all known bigyromonads are exclusively marine. Molecular clock

565   analyses indicate the Silurian period as the time of oomycete origins (Matari and Blair, 2014),

566   while the earliest fossil evidence points to the Devonian period (Krings et al., 2011). The fossil

567   evidence of the early diverging genera have shown them to be marine parasites of seaweed, or

568   of crustaceans based on molecular studies (Beakes and Sekimoto, 2009), both suggesting a

569   marine origin of oomycetes as a facultative parasitic osmotroph (Beakes et al., 2014, 2012;

570   Beakes and Thines, 2017).

571   The origin and evolution of major stramenopile subgroups is coming into sharper focus

572   with the increase in phylogenomic data from diverse species. The new taxa described here,

573   together with future descriptions of the still-substantial diversity of bigyromonada that has not

574   been well-characterized, can potentially shed more light on this and the origins of oomycetes in

575   particular. We propose that the ancestor of oomycetes was a phagoheterotrophic amoeboid, as

576   postulated in the evolution of true fungi (Zmitrovich, 2018), and that this transition might be

577   better understood through a detailed functional examination of the novel species. Just as the

578   highly successful analyses of choanoflagellates and unicellular opisthokonts changed our

579   understanding of the origin of animals (Chow et al., 2019; Sebé-Pedrós et al., 2013), a similar

580   analysis of the distribution of genes involved in Pseudofungi cell-aggregation or pseudopodia

581   formation across the diversity of bigyromonads could be a future direction to understand the

582   evolution of these unique phagoheterotrophs and oomycetes.

583

584   TAXONOMIC SUMMARY

585

586   Taxonomy: Eukaryota; SAR Burki et al. 2008, emend. Adl et al. 2012; Stramenopiles Patterson

587   1989, emend. Adl et al. 2005; Gyrista Cavalier-Smith 1998; Bigyromonadea Cavalier-Smith, T.

588   1998; Developea Karpov et Aleoshin 2016 *Cubaremonas* n. gen. Tikhonenkov, Cho, and

589   Keeling

590   Diagnosis: naked and solitary bacteriovorous protist. Cell shape is irregularly ovoid, with the

591   convex dorsal side and the flatter ventral side. Cells possess two heterodynamic flagella

592   emerging from a conspicuous ventral depression, which starts from the anterior end and

593   continues ventrally to the middle of the cell. In culture condition, the cells predominantly lie at

594   the bottom unattached with both flagella directed backward.

595   Etymology: from lat. cubare – to lie, to be lying down and monas (lat.) – unicellular organism.

596   Zoobank Registration. urn:lsid:zoobank.org:act:xxxxx

597   Type species. *Cubaremonas variflagellatum*

598   *Cubaremonas variflagellatum* n. sp. Tikhonenkov, Cho, and Keeling

599   Diagnosis: cells length 3.7 - 8 μm, cell width 2.6 - 5.4 μm. Flagella of unequal length, the

600   anterior one is approximately equal to the cell length while the posterior flagellum is 1.5 - 1.8

601   times longer than the cell. At lying cells, posterior flagellum runs along the ventral surface of the

602   cell and beats rapidly with sinusoidal pattern to draw water through the depression. The anterior

603   flagellum is hook-shaped and sweeps slowly down behind the posterior flagellum. Starving cells

604   have a small rostrum at the anterior end. Digestive vacuole is situated at the cell posterior. An

605   observed cell division produces two or four cells.

606   Type Figure: Fig. 4X illustrates a live cell of strain Dev-1.

607   Gene sequence: The SSU rRNA gene sequence has the GenBank Accession Number XXXXX.

608   Type locality: water column of Strait of Georgia, British Columbia, Canada

609   Etymology: the species name means "unequal flagella", lat.

610   Zoobank Registration: urn:lsid:zoobank.org:act:XXXXXXXX

611

612   *Develocanicus* n. gen. Tikhonenkov, Cho, Mylnikov, and Keeling

613   Diagnosis: Free-swimming naked eukaryovorous heterokont flagellates with two non-

614   acronematic heterodynamic flagella of unequal lengths. The shape of the cell is irregularly

615   flattened ellipse, where the dorsal side is more convex, and the ventral side is flatter. Flagella

616   emerge from a prominent ventral depression which passes into a shallow wide groove along the

617   entire length of the cell.

618   Etymology: from développé (fr.) – characteristic ballet movement and volcanicus (lat.) (found

619   near volcanos in Kanary island and Crimea).

620   Zoobank Registration. urn:lsid:zoobank.org:act:xxxxx

621   Type species. *Develocanicus komovi*

622

623   *Develocanicus komovi* n. sp. Tikhonenkov, Cho, Mylnikov, and Keeling

624   Diagnosis: cell length 5.4 - 10 μm, cell width 3.8 - 7.4 μm. The posterior flagellum is two times

625   longer than the cell, the anterior flagellum is approximately 1 - 1.5 times longer. Cells swim

626   without rotation. At that, posterior flagellum is directed backward and straight, running along the

627   ventral cell of the cell. Anterior flagellum beats rapidly and is directed forward while slightly

628   curved. Medial nucleus is located closer to the dorsal side of the cell. Large digestive vacuole is

629   situated at the posterior part of the cell. Cells can form pseudopodia and aggregations and attach

630   to each other. Transverse binary fission.

631   Type Figure: Fig. 4C illustrates a live cell of strain Colp-23.

632   Gene sequence: The SSU rRNA gene sequence has the GenBank Accession Number XXXXX.

633   Type locality: black volcanic sand on the littoral of Maria Jimenez Beach (Playa Maria Jiménez),

634   Puerto de la Cruz, Tenerife, Spain

635 Etymology: named after Prof., Dr. Viktor T. Komov, Russian ecotoxicologist, who carried out

636 fieldwork and collect samples, where new species was discovered.

637 Zoobank Registration: urn:lsid:zoobank.org:act:XXXXXXXX

638

639 *Develocanicus vyazemskyi* n. sp. Tikhonenkov, Cho, Mylnikov, and Keeling

640 Diagnosis: cell 7.4 - 12.5 μm long, 4.8 - 9.2 μm wide. The posterior flagellum is two times

641 longer than the cell, the anterior flagellum is approximately 1 - 1.5 times longer. Cells swim

642 without rotation. At that, posterior flagellum is directed backward and straight, running along the

643 ventral cell of the cell. Anterior flagellum beats rapidly and is directed forward while slightly

644 curved. In non-motile cells, both flagella are directed backward, beating in a slow sinusoidal

645 wave. Medial nucleus is located closer to the dorsal side of the cell. Large digestive vacuole is

646 situated at the posterior part of the cell. Transverse binary fission.

647 Type Figure: Fig. 4A illustrates a live cell of strain Colp-30.

648 Gene sequence: The SSU rRNA gene sequence has the GenBank Accession Number XXXXX.

649 Type locality: near shore sediments on the littoral near T.I. Vyazemsky Karadag Scientific

650 Station, Crimea

651 Etymology: named after Dr. T.I. Vyazemsky, founder and first director of Karadag Scientific

652 Station, Crimea

653 Zoobank Registration: urn:lsid:zoobank.org:act:XXXXXXXX

654

655 *Develocauda* n. gen. Tikhonenkov, Cho, and Keeling

656   Diagnosis: Free-swimming eukaryovorous heterokont flagellates with slightly flattened

657   elongated-oval cells and two heterodynamic flagella. The anterior end is more rounded, the

658   posterior end of the cell can be pointed, forming a characteristic "tail" in starving cells. Flagella

659   emerge from a pronounced deep ventral depression, which almost extends to the dorsal side of

660   the cell. Depression transforms into a shallow groove spanning along the entire cell, in which the

661   posterior flagellum can fit.

662   Etymology: from développé (fr.) – characteristic ballet movement and cauda (lat.) – tail.

663   Zoobank Registration. urn:lsid:zoobank.org:act:xxxxx

664   Type species. *Develocauda condao*

665

666

667   *Develocauda condao* n. sp. Tikhonenkov, Cho, and Keeling

668   Cell length 5.14 - 12 μm, width 2.8 - 5.42 μm. The caudal extension is about 4.57 x 1.42 μm in

669   size. Flagella of almost equal length. The cells swim very quickly without rotating along the

670   longitudinal axis. The posterior flagellum is straight and directed backwards. The anterior

671   flagellum is directed forward, beats actively, and is only slightly curved. Cells can be partially

672   fused and aggregated. Medial nucleus is located closer to the dorsal side of the cell. Transverse

673   binary fission.

674   Type Figure: Fig. 4N illustrates a live cell of strain Colp-29.

675   Gene sequence: The SSU rRNA gene sequence has the GenBank Accession Number XXXXX.

676   Type locality: near shore sediments on the littoral of north-east part of Con Dao Island, South

677   Vietnam

678   Etymology: named after Con Dao Island, South Vietnam, where species was discovered.

679   Zoobank Registration: urn:lsid:zoobank.org:act:XXXXXXXX

680

681   Pirsoniales Cavalier-Smith 1998, emend. 2006

682   Studied pirsoniales most likely represent a motile zoospore stages of unknown algal parasites.

683   Since data on the stage of the parasitic trophonts (auxosome and a trophosome) are not available,

684   it is premature to formulate taxonomic diagnoses. But we provide provisional names (nom.

685   prov.) which can be used for future research.

686   *Pirsonia chemainus* nom. prov. Tikhonenkov, Cho, and Keeling

687   Etymology: species epithet is after the Stz'uminus First Nation traditional territory (Strait of

688   Georgia area) claimed by the Chemainus First Nation

689   Type locality: water column of the Strait of Georgia, British Columbia, Canada

690   Gene sequence: The SSU rRNA gene sequence has the GenBank Accession Number XXXXX.

691   *Koktebelia satura* nom. prov. Tikhonenkov, Cho, and Keeling

692   Etymology: genus epithet reflects the place of finding, Koktebel bay, Crimea; species epithet –

693   from satur (lat.), well-fed.

694   Type locality: near shore sediments on the littoral near T.I. Vyazemsky Karadag Scientific

695   Station, Crimea

696   Gene sequence: The SSU rRNA gene sequence has the GenBank Accession Number XXXXX.

697

698   *Feodosia pseudopoda* nom. prov. Tikhonenkov, Cho, and Keeling

699   Etymology: genus epithet reflects the place of finding, the settlement Beregovoye, Feodosiya,

700   Crimea; species epithet reflects the ability to produce pseudopodia.

701   Type locality: near shore sand on the littoral of the beach in the settlement Beregovoye,

702   Feodosiya, Crimea

703   Gene sequence: The SSU rRNA gene sequence has the GenBank Accession Number XXXXX.

704

705

706 **Acknowledgements**

716   **References**

717   Aleoshin, V. V., Mylnikov, A.P., Mirzaeva, G.S., Mikhailov, K. V., Karpov, S.A., 2016.

718   Heterokont predator Develorapax marinus gen. et sp. nov. - A model of the ochrophyte

719   ancestor. Front. Microbiol. 7, 1–14. https://doi.org/10.3389/fmicb.2016.01194

720   Ali, R.H., Bogusz, M., Whelan, S., Tamura, K., 2019. Identifying Clusters of High Confidence

721   Homologies in Multiple Sequence Alignments. Mol. Biol. Evol. 36, 2340–2351.

722   https://doi.org/10.1093/molbev/msz142

723   Altschul, S.F., Gish, W., Miller, W., Myers, E.W., Lipman, D.J., 1990. Basic Local Alignment

724   Search Tool. J. Mol. Biol. 215, 403–410. https://doi.org/10.1016/S0022-2836(05)80360-2

725   Anderson, O.R., Cavalier-Smith, T., 2012. Ultrastructure of Diplophrys parva, a new small

726   freshwater species, and a revised analysis of Labyrinthulea (Heterokonta). Acta Protozool.

727   51, 291–304. https://doi.org/10.4467/16890027AP.12.023.0783

728   Andrews, S., 2010. FastQC: A quality control tool for high throughput sequence data.

729   Bassani, I., Rancurel, C., Pagnotta, S., Orange, F., Pons, N., Lebrigand, K., Panabières, F.,

730   Counillon, L., Noblin, X., Galiana, E., 2020. Transcriptomic and ultrastructural signatures

731   of k+-induced aggregation in phytophthora parasitica zoospores. Microorganisms 8, 1–18.

732   https://doi.org/10.3390/microorganisms8071012

733   Bateman, A., Martin, M.J., Orchard, S., Magrane, M., Agivetova, R., Ahmad, S., Alpi, E.,

734   Bowler-Barnett, E.H., Britto, R., Bursteinas, B., Bye-A-Jee, H., Coetzee, R., Cukura, A.,

735   Silva, A. Da, Denny, P., Dogan, T., Ebenezer, T.G., Fan, J., Castro, L.G., Garmiri, P.,

736   Georghiou, G., Gonzales, L., Hatton-Ellis, E., Hussein, A., Ignatchenko, A., Insana, G.,

737   Ishtiaq, R., Jokinen, P., Joshi, V., Jyothi, D., Lock, A., Lopez, R., Luciani, A., Luo, J.,

738   Lussi, Y., MacDougall, A., Madeira, F., Mahmoudy, M., Menchi, M., Mishra, A., Moulang,

739   K., Nightingale, A., Oliveira, C.S., Pundir, S., Qi, G., Raj, S., Rice, D., Lopez, M.R., Saidi,

740   R., Sampson, J., Sawford, T., Speretta, E., Turner, E., Tyagi, N., Vasudev, P., Volynkin, V.,

741   Warner, K., Watkins, X., Zaru, R., Zellner, H., Bridge, A., Poux, S., Redaschi, N., Aimo,

742   L., Argoud-Puy, G., Auchincloss, A., Axelsen, K., Bansal, P., Baratin, D., Blatter, M.C.,

743   Bolleman, J., Boutet, E., Breuza, L., Casals-Casas, C., de Castro, E., Echioukh, K.C.,

744   Coudert, E., Cuche, B., Doche, M., Dornevil, D., Estreicher, A., Famiglietti, M.L.,

745   Feuermann, M., Gasteiger, E., Gehant, S., Gerritsen, V., Gos, A., Gruaz-Gumowski, N.,

746   Hinz, U., Hulo, C., Hyka-Nouspikel, N., Jungo, F., Keller, G., Kerhornou, A., Lara, V., Le

747   Mercier, P., Lieberherr, D., Lombardot, T., Martin, X., Masson, P., Morgat, A., Neto, T.B.,

748   Paesano, S., Pedruzzi, I., Pilbout, S., Pourcel, L., Pozzato, M., Pruess, M., Rivoire, C.,

749   Sigrist, C., Sonesson, K., Stutz, A., Sundaram, S., Tognolli, M., Verbregue, L., Wu, C.H.,

750   Arighi, C.N., Arminski, L., Chen, C., Chen, Y., Garavelli, J.S., Huang, H., Laiho, K.,

751   McGarvey, P., Natale, D.A., Ross, K., Vinayaka, C.R., Wang, Q., Wang, Y., Yeh, L.S.,

752   Zhang, J., 2021. UniProt: The universal protein knowledgebase in 2021. Nucleic Acids Res.

753   49, D480–D489. https://doi.org/10.1093/nar/gkaa1100

754   Beakes, G.W., Glockling, S.L., Sekimoto, S., 2012. The evolutionary phylogeny of the oomycete

755   "fungi." Protoplasma 249, 3–19. https://doi.org/10.1007/s00709-011-0269-2

756   Beakes, G.W., Honda, D., Thines, M., 2014. Systematics of the Straminipila:

757   Labyrinthulomycota, Hyphochytriomycota, and Oomycota, in: Esser, K., McLaughlin, D.J.,

758   Spatafora, J.W. (Eds.), The Mycota, Vol. VIIA. Fungal Taxonomy and Systematics.

759   Springer Verlag, Germany, pp. 39–97. https://doi.org/10.1007/978-3-642-55318-9

760   Beakes, G.W., Sekimoto, S., 2009. The evolutionary phylogeny of oomycetes - insights gained

761   from studies of holocarpic parasites of algae and invertebrates, in: Lamour, K., Kamoun, S.

762   (Eds.), Oomycete Genetics and Genomics: Diversity, Interactions, and Research Tools.

763   John Wiley & Sons, Inc, USA, pp. 1–24. https://doi.org/10.1002/9780470475898.ch1

764   Beakes, G.W., Thines, M., 2017. Hyphochytriomycota and Oomycota., in: Archibald, J.M.,

765   Slamovits, C.H., Simpson, A.G.B., Margulis, L., Melkonian, M., Chapman, D.J., Corliss,

766   J.O. (Eds.), Handbook of the Protists. Springer Verlag, Cham, Switzerland, pp. 435–505.

767   Bendtsen, J.D., Nielsen, H., Von Heijne, G., Brunak, S., 2004. Improved prediction of signal

768   peptides: SignalP 3.0. J. Mol. Biol. 340, 783–795.

769   https://doi.org/10.1016/j.jmb.2004.05.028

770   Bessey, E.A., 1950. Hyphochytriales, in: Morphology and Taxonomy of Fungi. The Blakiston

771   Company, Philadelphia, PA, USA, p. 675.

772   Bolger, A.M., Lohse, M., Usadel, B., 2014. Trimmomatic: A flexible trimmer for Illumina

773   sequence data. Bioinformatics 30, 2114–2120.

774   https://doi.org/10.1093/bioinformatics/btu170

775   Brown, M.W., Kolisko, M., Silberman, J.D., Roger, A.J., 2012. Aggregative multicellularity

776   evolved independently in the eukaryotic supergroup Rhizaria. Curr. Biol. 22, 1123–1127.

777   https://doi.org/10.1016/j.cub.2012.04.021

778   Burki, F., Kaplan, M., Tikhonenkov, D. V., Zlatogursky, V., Minh, B.Q., Radaykina, L. V.,

779   Smirnov, A., Mylnikov, A.P., Keeling, P.J., 2016. Untangling the early diversification of

780   eukaryotes: A phylogenomic study of the evolutionary origins of centrohelida, haptophyta

781   and cryptista. Proc. R. Soc. B Biol. Sci. 283. https://doi.org/10.1098/rspb.2015.2802

782   Capella-Gutiérrez, S., Silla-Martínez, J.M., Gabaldón, T., 2009. trimAl: A tool for automated

783   alignment trimming in large-scale phylogenetic analyses. Bioinformatics 25, 1972–1973.

784   https://doi.org/10.1093/bioinformatics/btp348

785   Cavalier-Smith, T., 1998. A revised six-kingdom system of life. Biol. Rev. Camb. Philos. Soc.

786   73, 203–266. https://doi.org/10.1017/s0006323198005167

787   Cavalier-Smith, T., Chao, E.E.Y., 2006. Phylogeny and megasystematics of phagotrophic

788   heterokonts (kingdom Chromista). J. Mol. Evol. 62, 388–420.

789   https://doi.org/10.1007/s00239-004-0353-8

790   Cavalier-Smith, T., Lewis, R., Chao, E.E., Oates, B., Bass, D., 2009. Helkesimastix marina n. sp.

791   (Cercozoa: Sainouroidea superfam. n.) a Gliding Zooflagellate of Novel Ultrastructure and

792   Unusual Ciliary Behaviour. Protist 160, 452–479.

793   https://doi.org/10.1016/j.protis.2009.03.003

794   Cavalier-Smith, T., Scoble, J.M., 2013a. Phylogeny of Heterokonta: Incisomonas marina, a

795   uniciliate gliding opalozoan related to Solenicola (Nanomonadea), and evidence that

796   Actinophryida evolved from raphidophytes. Eur. J. Protistol. 49, 328–353.

797   https://doi.org/10.1016/j.ejop.2012.09.002

798   Cavalier-Smith, T., Scoble, J.M., 2013b. Phylogeny of Heterokonta: Incisomonas marina, a

799   uniciliate gliding opalozoan related to Solenicola (Nanomonadea), and evidence that

800   Actinophryida evolved from raphidophytes. Eur. J. Protistol. 49, 328–353.

801   https://doi.org/10.1016/j.ejop.2012.09.002

802   Chow, J., Dionne, H.M., Prabhakar, A., Mehrotra, A., Somboonthum, J., Gonzalez, B., Edgerton,

803   M., Cullen, P.J., 2019. Aggregate Filamentous Growth Responses in Yeast. mSphere 4, 1–

804   25. https://doi.org/10.1128/msphere.00702-18

805   de Vargas, Colomban, Audic, S., Henry, N., Decelle, J., Mahe, F., Logares, R., Lara, E., Berney,

806   C., Le Bescot, N., Probert, I., Carmichael, M., Poulain, J., Romac, S., Colin, S., Aury, J.-M.,

807   Bittner, L., Chaffron, S., Dunthorn, M., Engelen, S., Flegontova, O., Guidi, L., Horak, A.,

808   Jaillon, O., Lima-Mendez, G., Lukes, J., Malviya, S., Morard, R., Mulot, M., Scalco, E.,

809   Siano, R., Vincent, F., Zingone, A., Dimier, C., Coordinators, T.O., Picheral, M., Searson,

810   S., Kandels-Lewis, S., Acinas, S.G., Bork, P., Bowler, C., Gorsky, G., Grimsley, N.,

811   Hingamp, P., Iudicone, D., Not, F., Ogata, H., Pesant, S., Raes, J., Sieracki, M.E., Speich,

812   S., Stemmann, L., Sunagawa, S., Weissenbach, J., Wincker, P., Karsenti, E., 2015.

813   Eukaryotic plankton diversity in the sunlit ocean. Science (80-.). 348, 1261605–1/11.

814   https://doi.org/10.1126/science.1261605

815 Del Campo, J., Not, F., Forn, I., Sieracki, M.E., Massana, R., 2013. Taming the smallest

816   predators of the oceans. ISME J. 7, 351–358. https://doi.org/10.1038/ismej.2012.85

817 Delsuc, F., Brinkmann, H., Philippe, H., 2005. Phylogenomics and the reconstruction of the tree

818   of life. Nat. Rev. Genet. 6, 361–375. https://doi.org/10.1038/nrg1603

819 Derelle, R., López-García, P., Timpano, H., Moreira, D., 2016. A Phylogenomic Framework to

820   Study the Diversity and Evolution of Stramenopiles (=Heterokonts). Mol. Biol. Evol. 33,

821   2890–2898. https://doi.org/10.1093/molbev/msw168

822 Dick, M.W., 2000. Straminipilous fungi: systematics of the peronosporomycetes, including

823   accounts of the marine straminipilous portests, the plasmodiophorids, and similar

824   organisms, 1st ed. Spring Netherlands, Netherlands. https://doi.org/10.1007/978-94-015-

825   9733-3

826 Du, Q., Kawabe, Y., Schilde, C., Chen, Z.H., Schaap, P., 2015. The Evolution of Aggregative

827   Multicellularity and Cell-Cell Communication in the Dictyostelia. J. Mol. Biol. 427, 3722–

828   3733. https://doi.org/10.1016/j.jmb.2015.08.008

829 Dykstra, M.J., Olive, L.S., Mycologia, S., Aug, J., Aug, N.J., Dykstra, M.J., Olive, L.S., 1975.

830   Sorodiplophrys : An Unusual Sorocarp-Producing Protist. Mycologia 67, 873–879.

831   https://doi.org/10.2307/3758346

832   Galiana, E., Fourré, S., Engler, G., 2008. Phytophthora parasitica biofilm formation: Installation

833   and organization of microcolonies on the surface of a host plant. Environ. Microbiol. 10,

834   2164–2171. https://doi.org/10.1111/j.1462-2920.2008.01619.x

835   Gomaa, F., Mitchell, E.A.D., Lara, E., 2013. Amphitremida (Poche, 1913) Is a New Major,

836   Ubiquitous Labyrinthulomycete Clade. PLoS One 8.

837   https://doi.org/10.1371/journal.pone.0053046

838   Grabherr, M.G., Haas, B.J., Yassour, M., Levin, J.Z., Thompson, D.A., Amit, I., Adiconis, X.,

839   Fan, L., Raychowdhury, R., Zeng, Q., Chen, Z., Mauceli, E., Hacohen, N., Gnirke, A.,

840   Rhind, N., Di Palma, F., Birren, B.W., Nusbaum, C., Lindblad-Toh, K., Friedman, N.,

841   Regev, A., 2011. Full-length transcriptome assembly from RNA-Seq data without a

842   reference genome. Nat. Biotechnol. 29, 644–652. https://doi.org/10.1038/nbt.1883

843   Graupner, N., Jensen, M., Bock, C., Marks, S., Rahmann, S., Beisser, D., Boenigk, J., 2018.

844   Evolution of heterotrophy in chrysophytes as reflected by comparative transcriptomics.

845   FEMS Microbiol. Ecol. 94, 1–11. https://doi.org/10.1093/femsec/fiy039

846   Gruber-Vodicka, H.R., Seah, B.K.B., Pruesse, E., 2020. phyloFlash: Rapid Small-Subunit rRNA

847   Profiling and Targeted Assembly from Metagenomes. mSystems 5.

848   https://doi.org/10.1128/msystems.00920-20

849   Gruber, A., Rocap, G., Kroth, P.G., Armbrust, E.V., Mock, T., 2015. Plastid proteome prediction

850   for diatoms and other algae with secondary plastids of the red lineage. Plant J. 81, 519–528.

851   https://doi.org/10.1111/tpj.12734

852   Haas, B., 2015. TransDecoder (Find Coding Regions Within Transcripts) [WWW Document].

853   GitHub. URL https://github.com/TransDecoder/TransDecoder

854   Hackl, T., Martin, R., Barenhoff, K., Duponchel, S., Heider, D., Fischer, M.G., 2020. Four high-

855   quality draft genome assemblies of the marine heterotrophic nanoflagellate Cafeteria

856   roenbergensis. Sci. Data 7, 1–9. https://doi.org/10.1038/s41597-020-0363-4

857   Hehenberger, E., Gast, R.J., Keeling, P.J., 2019. A kleptoplastidic dinoflagellate and the tipping

858   point between transient and fully integrated plastid endosymbiosis. Proc. Natl. Acad. Sci. U.

859   S. A. 116, 17934–17942. https://doi.org/10.1073/pnas.1910121116

860   Hehenberger, E., Tikhonenkov, D. V., Kolisko, M., del Campo, J., Esaulov, A.S., Mylnikov,

861   A.P., Keeling, P.J., 2017. Novel Predators Reshape Holozoan Phylogeny and Reveal the

862   Presence of a Two-Component Signaling System in the Ancestor of Animals. Curr. Biol.

863   27, 2043-2050.e6. https://doi.org/10.1016/j.cub.2017.06.006

864   Hickman, C.J., 1970. Biology of Phytophthora Zoospores. Phytopathology.

865   https://doi.org/10.1094/phyto-60-1128

866   Ho, H.H., Hickman, C.J., 1967. Asexual Reproduction and Behavior of Zoospores of

867   Phytophthora Megasperma Var. Sojae. Can. J. Bot. 45, 1963–1981.

868   https://doi.org/10.1139/b67-215

869   Irwin, N.A.T., 2021. Phylogenomic-analysis [WWW Document]. GitHub. URL

870   https://github.com/nickatirwin/Phylogenomic-analysis (accessed 7.6.21).

871   Judelson, H.S., Blanco, F.A., 2005. The spores of Phytophthora: Weapons of the plant destroyer.

872   Nat. Rev. Microbiol. 3, 47–58. https://doi.org/10.1038/nrmicro1064

873   Kalyaanamoorthy, S., Minh, B.Q., Wong, T.K.F., Haeseler, A. Von, Jermiin, L.S., 2017.

874   ModelFinder : fast model selection for accurate phylogenetic estimates. Nat. Methods 14.

875   https://doi.org/10.1038/nmeth.4285

876   Kapli, P., Yang, Z., Telford, M.J., 2020. Phylogenetic tree building in the genomic age. Nat.

877   Rev. Genet. 21, 428–444. https://doi.org/10.1038/s41576-020-0233-0

878   Katoh, K., Standley, D.M., 2013. MAFFT multiple sequence alignment software version 7:

879   Improvements in performance and usability. Mol. Biol. Evol. 30, 772–780.

880   https://doi.org/10.1093/molbev/mst010

881   Keeling, P.J., 2002. Molecular phylogenetic position of Trichomitopsis termopsidis (Parabasalia)

882   and evidence for the Trichomitopsiinae. Eur. J. Protistol. 38, 279–286.

883   https://doi.org/10.1078/0932-4739-00874

884   Keeling, P.J., Burki, F., 2019. Progress towards the Tree of Eukaryotes. Curr. Biol. 29, R808–

885   R817. https://doi.org/10.1016/j.cub.2019.07.031

886   Keeling, P.J., Burki, F., Wilcox, H.M., Allam, B., Allen, E.E., Amaral-Zettler, L.A., Armbrust,

887   E.V., Archibald, J.M., Bharti, A.K., Bell, C.J., Beszteri, B., Bidle, K.D., Cameron, C.T.,

888   Campbell, L., Caron, D.A., Cattolico, R.A., Collier, J.L., Coyne, K., Davy, S.K.,

889   Deschamps, P., Dyhrman, S.T., Edvardsen, B., Gates, R.D., Gobler, C.J., Greenwood, S.J.,

890   Guida, S.M., Jacobi, J.L., Jakobsen, K.S., James, E.R., Jenkins, B., John, U., Johnson,

891   M.D., Juhl, A.R., Kamp, A., Katz, L.A., Kiene, R., Kudryavtsev, A., Leander, B.S., Lin, S.,

892   Lovejoy, C., Lynn, D., Marchetti, A., McManus, G., Nedelcu, A.M., Menden-Deuer, S.,

893   Miceli, C., Mock, T., Montresor, M., Moran, M.A., Murray, S., Nadathur, G., Nagai, S.,

894   Ngam, P.B., Palenik, B., Pawlowski, J., Petroni, G., Piganeau, G., Posewitz, M.C.,

895   Rengefors, K., Romano, G., Rumpho, M.E., Rynearson, T., Schilling, K.B., Schroeder,

896   D.C., Simpson, A.G.B., Slamovits, C.H., Smith, D.R., Smith, G.J., Smith, S.R., Sosik,

897   H.M., Stief, P., Theriot, E., Twary, S.N., Umale, P.E., Vaulot, D., Wawrik, B., Wheeler,

898   G.L., Wilson, W.H., Xu, Y., Zingone, A., Worden, A.Z., 2014. The Marine Microbial

899   Eukaryote Transcriptome Sequencing Project (MMETSP): Illuminating the Functional

900   Diversity of Eukaryotic Life in the Oceans through Transcriptome Sequencing. PLoS Biol.

901   12, e1001889. https://doi.org/10.1371/journal.pbio.1001889

902   Ko, W.H., Chase, L.L., 1973. Aggregation of Zoospores of Phytophthora palmivora. J. Gen.

903   Microbiol. 78, 79–82. https://doi.org/10.1099/00221287-78-1-79

904   Kobert, K., Salichos, L., Rokas, A., Stamatakis, A., 2016. Computing the Internode Certainty

905   and Related Measures from Partial Gene Trees. Mol. Biol. Evol. 33, 1606–1617.

906   https://doi.org/10.1093/molbev/msw040

907   Kolodziej, K., Stoeck, T., 2007. Cellular identification of a novel uncultured marine

908   stramenopile (MAST-12 clade) small-subunit rRNA gene sequence from a Norwegian

909   estuary by use of fluorescence in situ hybridization-scanning electron microscopy. Appl.

910   Environ. Microbiol. 73, 2718–2726. https://doi.org/10.1128/AEM.02158-06

911   Krings, M., Taylor, T.N., Dotzler, N., 2011. The fossil record of the peronosporomycetes

912   (Oomycota). Mycologia 103, 445–457. https://doi.org/10.3852/10-278

913   Kühn, S., Medlin, L., Eller, G., Subunit, N.S., Dna, R., Kühn, S., Medlin, L., Eller, G., 2004.

914   Phylogenetic position of the parasitoid nanoflagellate *Pirsonia* inferred from nuclear-

915   encoded small subunit ribosomal DNA and a description of *Pseudopirsonia* n. gen. and

916   *Pseudopirsonia mucosa* (Drebes) comb.nov. Protist 155, 143–156.

917   https://doi.org/10.1078/143446104774199556

918   Laetsch, D.R., Blaxter, M.L., 2017. BlobTools : Interrogation of genome assemblies [version 1 ;

919   peer review : 2 approved with reservations]. F1000Research 6, 1–16.

920   https://doi.org/10.12688/f1000research.12232.1

921   Lartillot, N., Brinkmann, H., Philippe, H., 2007. Suppression of long-branch attraction artefacts

922   in the animal phylogeny using a site-heterogeneous model. BMC Evol. Biol. 7, 1–14.

923   https://doi.org/10.1186/1471-2148-7-S1-S4

924   Lartillot, N., Lepage, T., Blanquart, S., 2009. PhyloBayes 3: A Bayesian software package for

925   phylogenetic reconstruction and molecular dating. Bioinformatics 25, 2286–2288.

926   https://doi.org/10.1093/bioinformatics/btp368

927   Lartillot, N., Philippe, H., 2004. A Bayesian mixture model for across-site heterogeneities in the

928   amino-acid replacement process. Mol. Biol. Evol. 21, 1095–1109.

929   https://doi.org/10.1093/molbev/msh112

930   Leipe, D.D., Tong, S.M., Goggin, C.L., Slemenda, S.B., Pieniazek, N.J., Sogin, M.L., 1996. 16S-

931   like rDNA sequences from Developayella elegans, Labyrinthuloides haliotidis, and

932   Proteromonas lacertae confirm that the stramenopiles are a primarily heterotrophic group.

933   Eur. J. Protistol. 32, 449–458. https://doi.org/10.1016/S0932-4739(96)80004-6

934   Leonard, G., Labarre, A., Milner, D.S., Monier, A., Soanes, D., Wideman, J.G., Maguire, F.,

935   Stevens, S., Sain, D., Grau-Bové, X., Sebé-Pedrós, A., Stajich, J.E., Paszkiewicz, K.,

936   Brown, M.W., Hall, N., Wickstead, B., Richards, T.A., 2018. Comparative genomic

937   analysis of the 'pseudofungus 'Hyphochytrium catenoides. Open Biol. 8.

938   https://doi.org/10.1098/rsob.170184

939   Lin, Y.-C., Campbell, T., Chung, C.-C., Gong, G.-C., Chiang, K.-P., Worden, A.Z., 2012.

940   Distribution Patterns and Phylogeny of Marine Stramenopiles in the. Appl. Environ.

941   Microbiol. 3387–3399. https://doi.org/10.1128/AEM.06952-11

942   Massana, R., Campo, J., Sieracki, M.E., Audic, S., Logares, R., 2014. Exploring the uncultured

943   microeukaryote majority in the oceans : reevaluation of ribogroups within stramenopiles.

944   Int. Soc. Microb. Ecol. 8, 854–866. https://doi.org/10.1038/ismej.2013.204

945   Massana, R., Castresana, J., Balague, V., Guillou, L., Romari, K., Groisillier, A., Valentin, K.,

946   Pedros-Alio, C., 2004. Phylogenetic and Ecological Analysis of Novel Marine

947   Stramenopiles. Appl. Environ. Microbiol. 70, 3528–3534.

948   https://doi.org/10.1128/AEM.70.6.3528

949 Matari, N.H., Blair, J.E., 2014. A multilocus timescale for oomycete evolution estimated under

950   three distinct molecular clock models. BMC Evol. Biol. 14, 1–11.

951   https://doi.org/10.1186/1471-2148-14-101

952 Medlin, L., Elwood, H.J., Stickel, S., Sogin, M.L., 1988. The characterization of enzymatically

953   amplified eukaryotic 16S-like rRNA-coding regions. Gene 71, 491–499.

954   https://doi.org/10.1016/0378-1119(88)90066-2

955 Mitra, A., Flynn, K.J., Tillmann, U., Raven, J.A., Caron, D., Stoecker, D.K., Not, F., Hansen,

956   P.J., Hallegraeff, G., Sanders, R., Wilken, S., McManus, G., Johnson, M., Pitta, P., Våge,

957   S., Berge, T., Calbet, A., Thingstad, F., Jeong, H.J., Burkholder, J.A., Glibert, P.M.,

958   Granéli, E., Lundgren, V., 2016. Defining Planktonic Protist Functional Groups on

959   Mechanisms for Energy and Nutrient Acquisition: Incorporation of Diverse Mixotrophic

960   Strategies. Protist 167, 106–120. https://doi.org/10.1016/j.protis.2016.01.003

961 Nguyen, L.T., Schmidt, H.A., Von Haeseler, A., Minh, B.Q., 2015. IQ-TREE: A fast and

962   effective stochastic algorithm for estimating maximum-likelihood phylogenies. Mol. Biol.

963   Evol. 32, 268–274. https://doi.org/10.1093/molbev/msu300

964 Noguchi, F., Tanifuji, G., Brown, M.W., Fujikura, K., Takishita, K., 2016. Complex evolution of

965   two types of cardiolipin synthase in the eukaryotic lineage stramenopiles. Mol. Phylogenet.

966   Evol. 101, 133–141. https://doi.org/10.1016/j.ympev.2016.05.011

967 Parfrey, L.W., Lahr, D.J.G., 2013. Multicellularity arose several times in the evolution of

968   eukaryotes. BioEssays 35, 339–347. https://doi.org/DOI 10.1002/bies.201200143

969   Picelli, S., Faridani, O.R., Björklund, Å.K., Winberg, G., Sagasser, S., Sandberg, R., 2014. Full-

970   length RNA-seq from single cells using Smart-seq2. Nat. Protoc. 9, 171–181.

971   https://doi.org/10.1038/nprot.2014.006

972   Quang, L.S., Gascuel, O., Lartillot, N., 2008. Empirical profile mixture models for phylogenetic

973   reconstruction. Bioinformatics 24, 2317–2323.

974   https://doi.org/10.1093/bioinformatics/btn445

975   Quast, C., Pruesse, E., Yilmaz, P., Gerken, J., Schweer, T., Yarza, P., Peplies, J., Glöckner, F.O.,

976   2013. The SILVA ribosomal RNA gene database project: Improved data processing and

977   web-based tools. Nucleic Acids Res. 41, 590–596. https://doi.org/10.1093/nar/gks1219

978   Raghukumar, S., 1992. Bacterivory: a novel dual role for thraustochytrids in the sea. Mar. Biol.

979   113, 165–169. https://doi.org/10.1007/BF00367650

980   Richards, T.A., Talbot, N.J., 2013. Horizontal gene transfer in osmotrophs: playing with public

981   goods. Nat. Rev. Microbiol. 11, 720–727.

982   https://doi.org/http://dx.doi.org.ezproxy.library.ubc.ca/10.1038/nrmicro3108

983   Roure, B., Baurain, D., Philippe, H., 2013. Impact of missing data on phylogenies inferred from

984   empirical phylogenomic data sets. Mol. Biol. Evol. 30, 197–214.

985   https://doi.org/10.1093/molbev/mss208

986   Roure, B., Rodriguez-Ezpeleta, N., Philippe, H., 2007. SCaFoS: A tool for selection,

987   concatenation and fusion of sequences for phylogenomics. BMC Evol. Biol. 7, 1–12.

988   https://doi.org/10.1186/1471-2148-7-S1-S2

989   Roy, R.S., Price, D.C., Schliep, A., Cai, G., Korobeynikov, A., Yoon, H.S., Yang, E.C.,

990   Bhattacharya, D., 2014. Single cell genome analysis of an uncultured heterotrophic

991   stramenopile. Sci. Rep. 4, 1–8. https://doi.org/10.1038/srep04780

992   Savory, A.I.M., Grenville-Briggs, L.J., Wawra, S., Van West, P., Davidson, F.A., 2014. Auto-

993   aggregation in zoospores of Phytophthora infestans: The cooperative roles of bioconvection

994   and chemotaxis. J. R. Soc. Interface 11. https://doi.org/10.1098/rsif.2014.0017

995   Savory, F., Leonard, G., Richards, T.A., 2015. The Role of Horizontal Gene Transfer in the

996   Evolution of the Oomycetes. PLoS Pathog. 11, 1–6.

997   https://doi.org/10.1371/journal.ppat.1004805

998   Savory, F.R., Milner, D.S., Miles, D.C., Richards, T.A., 2018. Ancestral function and

999   diversification of a horizontally acquired oomycete carboxylic acid transporter. Mol. Biol.

1000   Evol. 35, 1887–1900. https://doi.org/10.1093/molbev/msy082

1001   Schnepf, E., Drebes, G., Elbrachter, M., 1990. *Pirsonia guinardiae* , gen. et spec. nov.: A

1002   parasitic flagellate on the marine diatom *Guinardia flaccida* with an unusual mode of food

1003   uptake. Helgolander Meeresunters 44, 275–293. https://doi.org/10.1007/BF02365468

1004   Schweikert, M., Schnepf, E., 1997. Light and electron microscopical observations on Pirsonia

1005   punctigerae spec. nov., a Nanoflagellate feeding on the marine centric diatom Thalassiosira

1006   punctigera. Eur. J. Protistol. 33, 168–177. https://doi.org/10.1016/S0932-4739(97)80033-8

1007   Sebé-Pedrós, A., Irimia, M., del Campo, J., Parra-Acero, H., Russ, C., Nusbaum, C., Blencowe,

1008   B.J., Ruiz-Trillo, I., 2013. Regulated aggregative multicellularity in a close unicellular

1009   relative of metazoa. Elife 2013, 1–20. https://doi.org/10.7554/eLife.01287

1010   Seeleuthner, Y., Mondy, S., Lombard, V., Carradec, Q., Pelletier, E., Wessner, M., Leconte, J.,

1011   Mangot, J.-F., Poulain, J., Labadie, K., Logares, R., Sunagawa, S., de Berardinis, V.,

1012   Salanoubat, M., Dimier, C., Kandels-Lewis, S., Picheral, M., Searson, S., Pesant, S.,

1013   Poulton, N., Stepanauskas, R., Bork, P., Bowler, C., Hingamp, P., Sullivan, M.B., Iudicone,

1014   D., Massana, R., Aury, J.-M., Henrissat, B., Karsenti, E., Jaillon, O., Sieracki, M., de

1015   Vargas, C., Wincker, P., 2018. Single-cell genomics of multiple uncultured stramenopiles

1016   reveals underestimated functional diversity across oceans. Nat. Commun. 9, 310.

1017   https://doi.org/10.1038/s41467-017-02235-3

1018   Seemann, T., 2007. Barrnap 0.9: BAsic Rapid Ribosomal RNA Predictor [WWW Document].

1019   GitHub. URL https://github.com/tseemann/barrnap

1020   Shimodaira, H., 2002. An approximately unbiased test of phylogenetic tree selection. Syst. Biol.

1021   51, 492–508. https://doi.org/10.1080/10635150290069913

1022   Shiratori, T., Nakayama, T., Ishida, K. ichiro, 2015. A New Deep-branching Stramenopile,

1023   Platysulcus tardus gen. nov., sp. nov. Protist 166, 337–348.

1024   https://doi.org/10.1016/j.protis.2015.05.001

1025   Shiratori, T., Thakur, R., Ishida, K., 2017. Pseudophyllomitus vesiculosus (Larsen and Patterson

1026   1990) Lee, 2002, a poorly studied phagotrophic biflagellate is the first characterized

1027   member of stramenoile environmental clade MAST-6. Protist 168, 439–451.

1028   https://doi.org/10.1016/j.protis.2017.06.004

1029   Sibbald, S.J., Archibald, J.M., 2017. More protist genomes needed. Nat. Ecol. Evol. 1, 1–3.

1030   https://doi.org/10.1038/s41559-017-0145

1031   Simão, F.A., Waterhouse, R.M., Ioannidis, P., Kriventseva, E. V., Zdobnov, E.M., 2015.

1032   BUSCO: Assessing genome assembly and annotation completeness with single-copy

1033   orthologs. Bioinformatics 31, 3210–3212. https://doi.org/10.1093/bioinformatics/btv351

1034   Stiller, J.W., Huang, J., Ding, Q., Tian, J., Goodwillie, C., 2009. Are algal genes in

1035   nonphotosynthetic protists evidence of historical plastid endosymbioses? BMC Genomics

1036   10, 484. https://doi.org/10.1186/1471-2164-10-484

1037   Sugimoto, H., Endoh, H., 2006. Analysis of fruiting body development in the aggregative ciliate

1038   Sorogena stoianovitchae (Ciliophora, Colpodea). J. Eukaryot. Microbiol. 53, 96–102.

1039   https://doi.org/10.1111/j.1550-7408.2005.00077.x

1040   Thakur, R., Shiratori, T., Ishida, K. ichiro, 2019. Taxon-rich Multigene Phylogenetic Analyses

1041   Resolve the Phylogenetic Relationship Among Deep-branching Stramenopiles. Protist 170,

1042   125682. https://doi.org/10.1016/j.protis.2019.125682

1043   Tikhonenkov, D. V., Janouškovec, J., Mylnikov, A.P., Mikhailov, K. V., Simdyanov, T.G.,

1044   Aleoshin, V. V., Keeling, P.J., 2014. Description of Colponema vietnamica sp.n. and

1045   Acavomonas peruviana n. gen. n. sp., Two New Alveolate Phyla (Colponemidia nom. nov.

1046   and Acavomonidia nom.nov.) and Their Contributions to Reconstructing the Ancestral State

1047   of Alveolates and Eukaryotes. PLoS One 9. https://doi.org/10.1371/journal.pone.0095467

1048   Tikhonenkov, D. V., Mazei, Y.A., Embulaeva, E.A., 2008. Degradation succession of

1049   heterotrophic flagellate communities in microcosms. Zh Obs. Biol 69, 57–64.

1050   Tikhonenkov, D. V, Janou, J., Keeling, P.J., Mylnikov, A.P., 2016. The Morphology ,

1051   Ultrastructure and SSU rRNA Gene Sequence of a New Freshwater Flagellate , Neobodo

1052   borokensis n . sp . (Kinetoplastea , Excavata). J. Eukaryot. Microbiol. 63, 220–232.

1053   https://doi.org/10.1111/jeu.12271

1054   Tong, S.M., 1995. Developayella elegans nov. gen., nov. spec., a New Type of Heterotrophic

1055   Flagellate from Marine Plankton. Eur. J. Protistol. 31, 24–31.

1056   https://doi.org/10.1016/S0932-4739(11)80352-4

1057   Torruella, G., Grau-Bové, X., Moreira, D., Karpov, S.A., Burns, J.A., Sebé-Pedrós, A., Völcker,

1058   E., López-García, P., 2018. Global transcriptome analysis of the aphelid Paraphelidium

1059   tribonemae supports the phagotrophic origin of fungi. Commun. Biol. 1, 1–11.

1060   https://doi.org/10.1038/s42003-018-0235-z

1061   Tsui, C.K.M., Marshall, W., Yokoyama, R., Honda, D., Lippmeier, J.C., Craven, K.D., Peterson,

1062   P.D., Berbee, M.L., 2009. Labyrinthulomycetes phylogeny and its implications for the

1063   evolutionary loss of chloroplasts and gain of ectoplasmic gliding. Mol. Phylogenet. Evol.

1064   50, 129–140. https://doi.org/10.1016/j.ympev.2008.09.027

1065   Tyler, B.M., Tripathy, S., Zhang, X., Dehal, P., Jiang, R.H.Y., Aerts, A., Arredondo, F.D.,

1066   Baxter, L., Bensasson, D., Beynon, J.L., Chapman, J., Damasceno, C.M.B., Dorrance, A.E.,

1067   Dou, D., Dickerman, A.W., Dubchak, I.L., Garbelotto, M., Gijzen, M., Gordon, S.G.,

1068   Govers, F., Grunwald, N.J., Huang, W., Ivors, K.L., Jones, R.W., Kamoun, S., Krampis, K.,

1069   Lamour, K.H., Lee, M.K., McDonald, W.H., Medina, M., Meijer, H.J.G., Nordberg, E.K.,

1070   Maclean, D.J., Ospina-Giraldo, M.D., Morris, P.F., Phuntumart, V., Putnam, N.H., Rash, S.,

1071   Rose, J.K.C., Sakihama, Y., Salamov, A.A., Savidor, A., Scheuring, C.F., Smith, B.M.,

1072   Sobral, B.W.S., Terry, A., Torto-Alalibo, T.A., Win, J., Xu, Z., Zhang, H., Grigoriev, I. V.,

1073   Rokhsar, D.S., Boore, J.L., 2006. Phytophthora genome sequences uncover evolutionary

1074   origins and mechanisms of pathogenesis. Science (80-.). 313, 1261–1266.

1075   https://doi.org/10.1126/science.1128796

1076   Wang, H.C., Minh, B.Q., Susko, E., Roger, A.J., 2018. Modeling Site Heterogeneity with

1077   Posterior Mean Site Frequency Profiles Accelerates Accurate Phylogenomic Estimation.

1078   Syst. Biol. 67, 216–235. https://doi.org/10.1093/sysbio/syx068

1079   Wang, Q., Sun, H., Huang, J., 2017. Re-analyses of "algal" genes suggest a complex

1080   evolutionary history of oomycetes. Front. Plant Sci. 8, 1–14.

1081   https://doi.org/10.3389/fpls.2017.01540

1082   Wawrzyniak, I., Courtine, D., Osman, M., Hubans-Pierlot, C., Cian, A., Nourrisson, C., Chabe,

1083   M., Poirier, P., Bart, A., Polonais, V., Delgado-Viscogliosi, P., El Alaoui, H., Belkorchia,

1084   A., van Gool, T., Tan, K.S.W., Ferreira, S., Viscogliosi, E., Delbac, F., 2015. Draft genome

1085   sequence of the intestinal parasite Blastocystis subtype 4-isolate WR1. Genomics Data 4,

1086   22–23. https://doi.org/10.1016/j.gdata.2015.01.009

1087   Weiler, B.A., Sa, E.L., Sieracki, M.E., Massana, R., del Campo, J., 2020. Mediocremonas

1088   mediterraneus ,a new member within the Developea. J. Eukaryot. Microbiol. 1, 0–2.

1089   https://doi.org/10.1111/jeu.12825

1090   Whelan, S., Irisarri, I., Burki, F., 2018. PREQUAL: Detecting non-homologous characters in sets

1091   of unaligned homologous sequences. Bioinformatics 34, 3929–3930.

1092   https://doi.org/10.1093/bioinformatics/bty448

1093   Yubuki, N., Pánek, T., Yabuki, A., Čepička, I., Takishita, K., Inagaki, Y., Leander, B.S., 2015.

1094   Morphological Identities of Two Different Marine Stramenopile Environmental Sequence

1095   Clades: Bicosoeca kenaiensis (Hilliard, 1971) and Cantina marsupialis (Larsen and

1096   Patterson, 1990) gen. nov., comb. nov. J. Eukaryot. Microbiol. 62, 532–542.

1097   https://doi.org/10.1111/jeu.12207

1098   Zheng, L., Mackrill, J.J., 2016. Calcium signaling in oomycetes: An evolutionary perspective.

1099   Front. Physiol. 7, 1–7. https://doi.org/10.3389/fphys.2016.00123

1100   Zhou, Y., Rodrigue, N., Lartillot, N., Philippe, H., 2007. Evaluation of the models handling

1101   heterotachy in phylogenetic inference. BMC Evol. Biol. 7, 1–13.

1102   https://doi.org/10.1186/1471-2148-7-206

1103   Zmitrovich, I. V, 2018. The Oomycota phenomenon, in: IV (XII) International Botanical

1104   Conference of Young Scientists. Mycology and lichenology, St. Petersburg, pp. 188–190.

1105

1106

1107
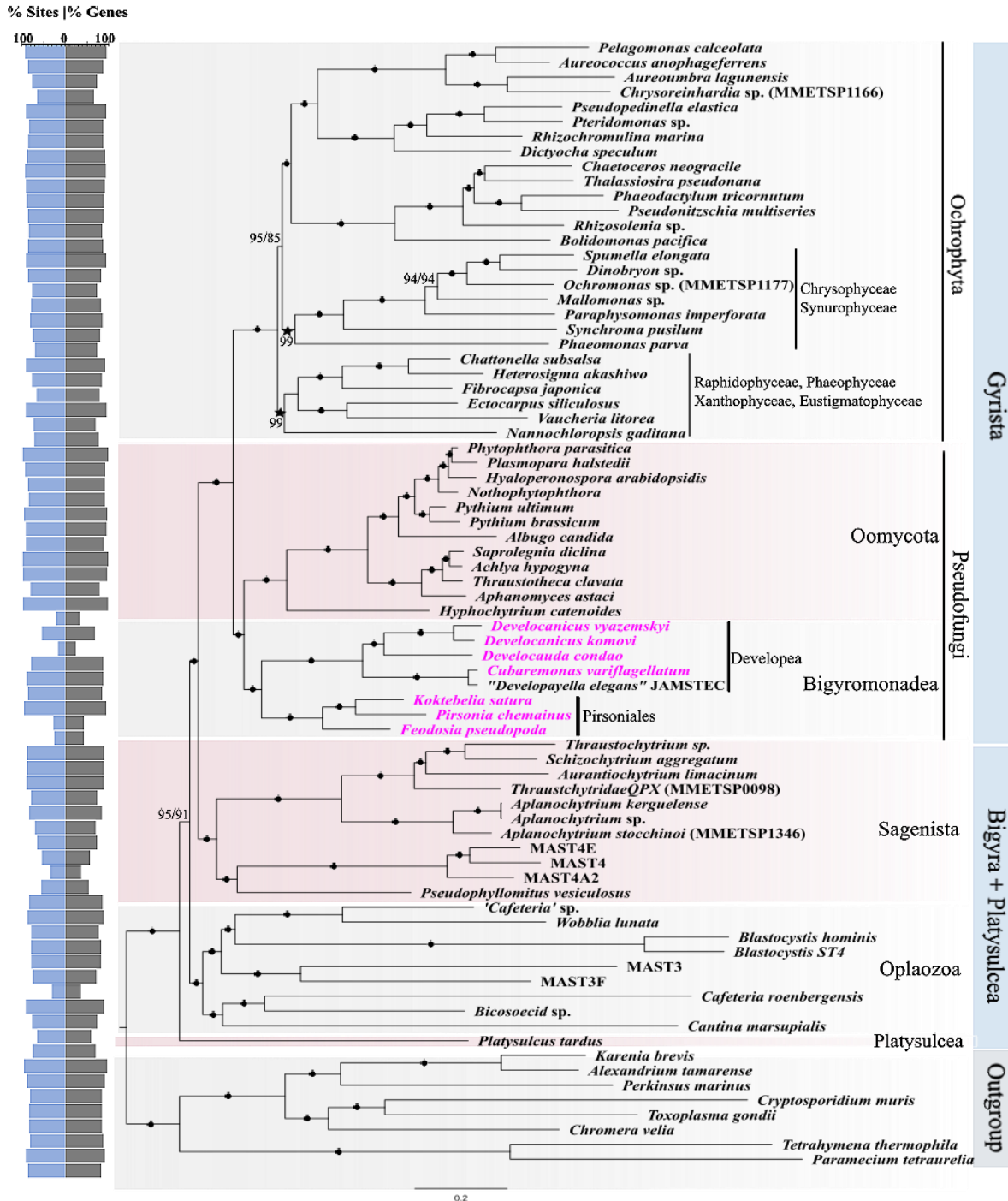
Figure 1. Multi-gene phylogenomic tree of stramenopiles with the seven new transcriptomes (pink) added to Gyrista, consisting of the concatenated alignments of 247 genes of 76 taxa. The tree was reconstructed using the Maximum-likelihood (ML) analysis, under the site-heterogenous model, LG+C60+F+G4+PMSF, implemented in IQ-Tree. Branch support was calculated using

1113   non-parametric PMSF 100 standard bootstrap (STB). Branches with ≥99% STB for both

1114   approaches are marked with black bullets while others are labelled as "Approach 1 STB/Approach

1115   2 STB". The topology of the trees generated from the two approaches were the same except the

1116   positions of Raphidophyceae, Phaeophyceae, Xanthophyceae + Eustigmatophacea and

1117   Chrysophyceae+Synurophceae, which were swapped in the tree reconstructed based on the dataset

1118   processed using approach 2 (i.e., Prequal/Divvier method); denoted by star symbols (Fig. S1). The

1119   percent sites (blue) and genes (grey) present for each transcriptome is depicted on the back-to-

1120   back bar plot on the left.

1121

1122
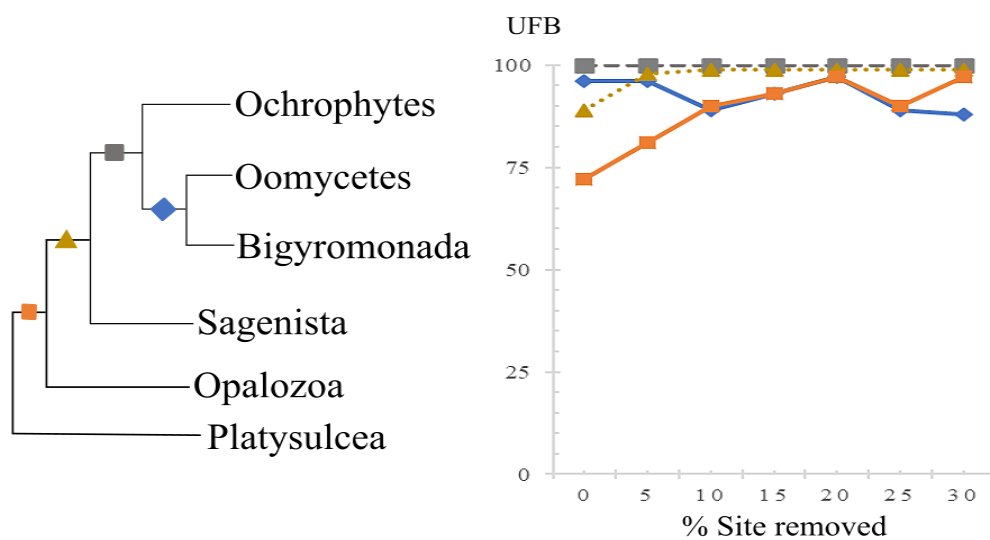
1123
1124   **Figure 2.** Summary of ultrafast bootstrap (UFB) with incremental removal of fast-evolving sites,

1125   based on the dataset processed with approach 1. Schematic representation the stramenopiles ML

1126   tree (left) with each branch marked with different shapes and colours. The line plot (right) showing

1127   the change in UFB for each branch when fast-evolving sites were incrementally removed by 5%.

1128   The monophyly of Gyrista shows full support throughout while the UFB increases incrementally

1129   for 'Sagenista' and 'Platysulcea'.

1130   Table 1. Approximately unbiased (AU) tests on tree constraints based on approach 1 dataset.

Approach 1 (MAFFT L-INS-i and trimAl -g 0.8)			
Constrained Tree	p-AU	logL	ΔlogL
Unconstrained ML tree	0.78	-3935691.338	0
ML tree	0.759	-3935691.338	0.00089261
Chain 1 (C+S+Pi),(R+P+X+E)	0.0541	-3935828.083	136.75
Chain 1 Modified (Bigyromonada+oomycetes)	0.267	-3935763.845	72.508
Chain 2 (C+S+Pi+E),(R+P+X)	**0.0297**	-3935859.39	168.05
Chain 2 Modified (Bigyromonada+oomycetes)	0.0924	-7871604.549	108.01
Chain 3 (R+P+X+E),(C+S)	**0.0119**	-3935874.998	183.66
Chain 3 Modified (Bigyromonada+oomycetes)	0.0717	-3935805.205	113.87
Chain 4 (C+S+E),(R+P+X)	**0.0186**	-3935860.003	168.67
Chain 4 Modified (Bigyromonada+oomycetes)	0.108	-3935765.741	74.404

1131   Except, the unconstrained ML tree, each tree was constrained under LG+C60+F+G4 using IQ-TREE with the
1132   approach 1 dataset. Chain 1 to chain 4 are generated from Bayesian analyses and contain
1133   (bigyromonada+ochrophytes). "Chain 1 Modified" to "Chain4 modified" contain hypothetical
1134   (bigyromonada+oomycetes) with the rest of topology remaining the same with their corresponding chains. Each
1135   unmodified chain is listed with different topology of Chyrisista as represented in Fig. S2. The unconstrained tree is
1136   based on ML tree reconstructed under LG+C60+F+G4+PMSF as presented in Fig. 1. The p-AU values were
1137   calculated using the AU test with 10,000 RELL bootstrap replicates, implemented in IQ-TREE. The maximum log
1138   likelihoods (logL) of each constrained and their differences (ΔlogL) compared to the unstrained tree are listed.
1139   Constraints with P-values lower than 0.05 are rejected, indicating confidence interval below 95% (marked bold).
1140   Raphidophyceae (R), Eustigmatophyceae (E), Chrysophyceae (C), Synurophyceae (S), Phaeophyceae (P),
1141   Pinguiophyceae (Pi), and Xanthophyceae (X).
1142
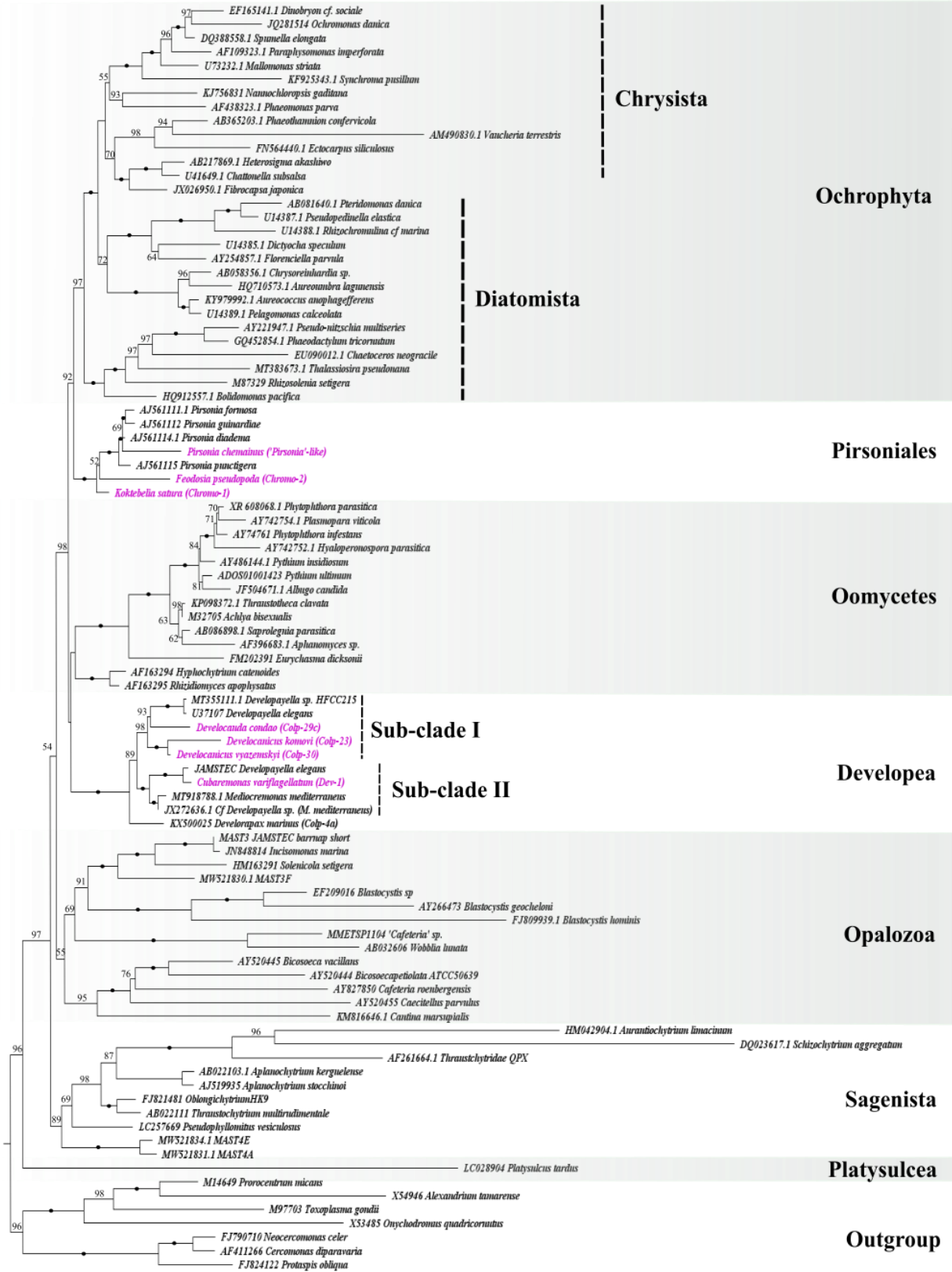
1144　**Figure 3.** ML tree reconstructed from a 18S rRNA gene alignment of 92 taxa (1650 sites), under

1145　BIC: TIM2+R6 with 1000 UFB. Branch support with ≥99% UFB is marked with black bullets

1146　while the values less than 50% are not shown. The seven new species described in this study are

1147　marked as pink: Pirsoniales forming a sisterhood with Ochrophytes and Developea forming a sister

1148　clade to Oomycetes. Within Developea, two previously assigned *Developayella* species

1149　(JAMSTEC transcriptome and the U37107 SSU rRNA sequence) are split into two sub-clades, in

1150　which the four novel Developea species are positioned.

1151
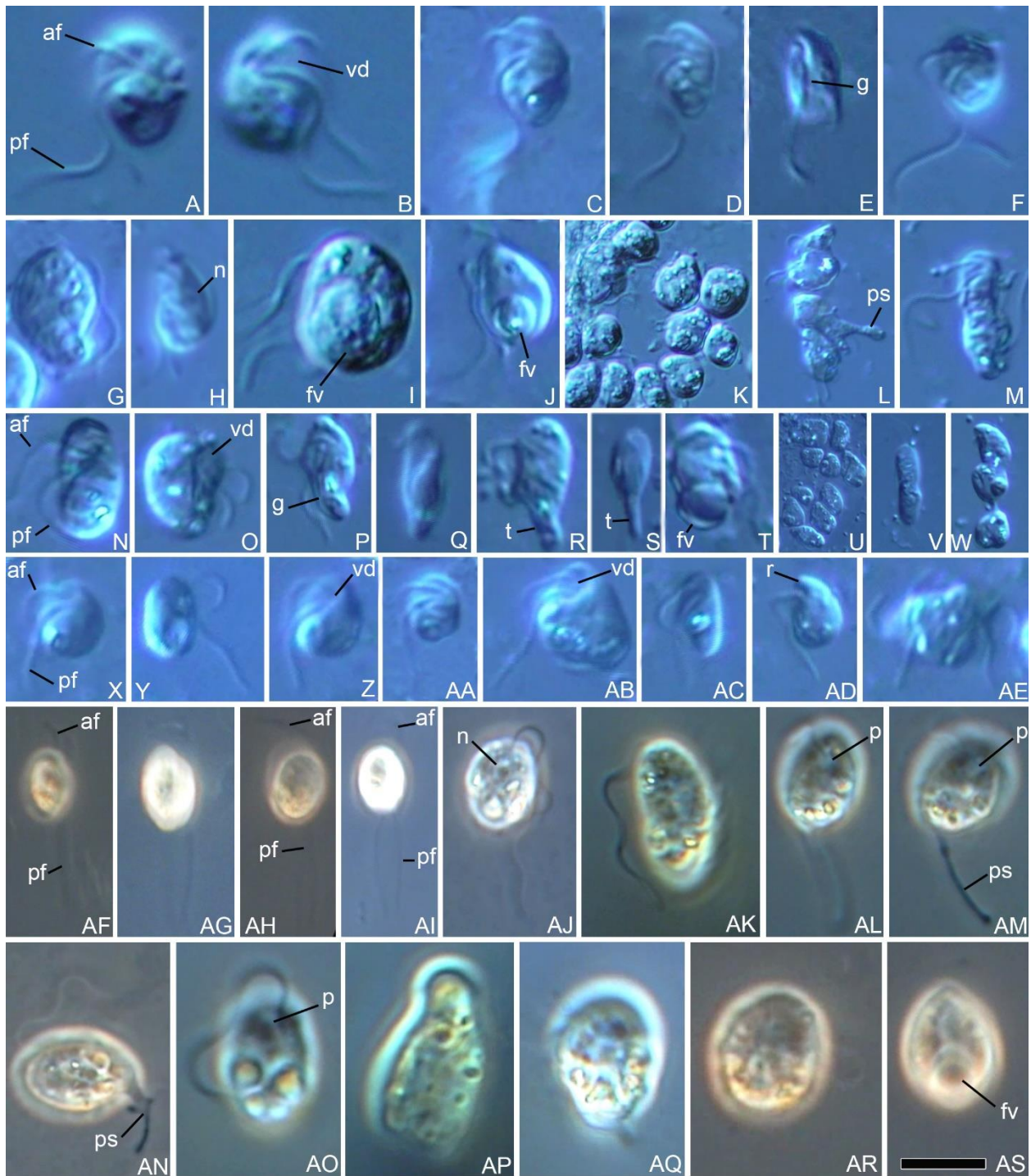
Figure 4. Morphology of novel phagoheterotrophic stramenopiles. **A, B.** *Develocanicus*

vyazemskyi, general cell view with flagella (anterior flagellum [af] and posterior flagellum [pf])

and ventral depression [vd]. **C–M.** *Develocanicus komovi,* C–F – general cell view with flagella

and ventral depression, shallow wide groove [g] is visible in (E), G – lying cell with posterior

1157   flagellum [pf] beating with a slow sinusoidal wave, H–J – cells with medial nucleus [n] (H) and

1158   large food vacuoles [fv] (I, J), K – cell aggregation, L – aggregated cells with pseudopodia [ps],

1159   M – transverse binary fission. **N–W.** *Develocauda condao,* N–P – general cell view with two

1160   flagella and ventral depression, Q – rod-shaped cell, R,S – cells with pointed 'tail-like' [t] posterior

1161   end, T – cells with large food vacuole, U – cell aggregation, V – transverse binary fission, W -

1162   partially fused cells. **X–AE.** *Cubaremonas variflagellatum,* X–AA – general cell view with

1163   flagella, AB – cell with conspicuous ventral depression, AC, AD – starving cells with small

1164   rostrum [r] (AD), AE – division into 4 cells. **AF, AG, AJ – AS.** *Feodosia pseudopoda,* AF, AG –

1165   typical fast swimming cell with two flagella, AJ, AK, AO – lying cells with sinusoid shaped

1166   flagella, AL–AN – cells with pseudopodia and anterior pit [p] (AL, AM), AP–AR – metabolic

1167   cells, AS – cell with large food vacuole. **AH.** *Koktebelia satura*, typical fast swimming cell with

1168   two flagella. **AI.** *Pirsonia chemainus*, typical fast swimming cell with two flagella. **Scale bar**: A,

1169   B, R, AK, AP, AQ, AS – 8 μm; C–H, J, N, P,Q, X–AA, AC, AD – 7 μm; I, O, T, AB – 5 μm; K,

1170   L, V, AF–AI – 15 μm; M, S, AE, AJ, AL–AO, AR – 10 μm; U – 25 μm; W – 20 μm.

1171
1172
1173

1174
1175

1176